

**Wave Amplitude and Intensity Measurement in Beams in the  
Presence of a Nearfield**

**H.M. El-Khatib, B.R. Mace and M.J. Brennan**

ISVR Technical Memorandum 909

February 2003



## SCIENTIFIC PUBLICATIONS BY THE ISVR

**Technical Reports** are published to promote timely dissemination of research results by ISVR personnel. This medium permits more detailed presentation than is usually acceptable for scientific journals. Responsibility for both the content and any opinions expressed rests entirely with the author(s).

**Technical Memoranda** are produced to enable the early or preliminary release of information by ISVR personnel where such release is deemed to be appropriate. Information contained in these memoranda may be incomplete, or form part of a continuing programme; this should be borne in mind when using or quoting from these documents.

**Contract Reports** are produced to record the results of scientific work carried out for sponsors, under contract. The ISVR treats these reports as confidential to sponsors and does not make them available for general circulation. Individual sponsors may, however, authorize subsequent release of the material.

## COPYRIGHT NOTICE

(c) ISVR University of Southampton      All rights reserved.

ISVR authorises you to view and download the Materials at this Web site ("Site") only for your personal, non-commercial use. This authorization is not a transfer of title in the Materials and copies of the Materials and is subject to the following restrictions: 1) you must retain, on all copies of the Materials downloaded, all copyright and other proprietary notices contained in the Materials; 2) you may not modify the Materials in any way or reproduce or publicly display, perform, or distribute or otherwise use them for any public or commercial purpose; and 3) you must not transfer the Materials to any other person unless you give them notice of, and they agree to accept, the obligations arising under these terms and conditions of use. You agree to abide by all additional restrictions displayed on the Site as it may be updated from time to time. This Site, including all Materials, is protected by worldwide copyright laws and treaty provisions. You agree to comply with all copyright laws worldwide in your use of this Site and to prevent any unauthorised copying of the Materials.

UNIVERSITY OF SOUTHAMPTON  
INSTITUTE OF SOUND AND VIBRATION RESEARCH  
DYNAMICS GROUP

**Wave Amplitude and Intensity Measurement  
in Beams in the Presence of a Nearfield**

by

**H.M. El-Khatib, B.R. Mace and M.J. Brennan**

ISVR Technical Memorandum No: 909

February 2003

Authorised for issue by  
Professor M.J. Brennan  
Group Chairman



## ABSTRACT

The vibrational behaviour of beams can be expressed by the propagating waves plus the nearfield ones. The propagating waves carry energy along the beam. The flow of this energy is called intensity. Usually nearfield (evanescent) waves don't carry energy.

In previous work, the amplitude of a positive-going propagating wave was estimated in real time in order to minimise the vibration level of a beam using feedforward active control.

In this project, both incident and reflected waves were estimated plus a positive-going nearfield one in real time.

Hence, instantaneous values of the response, internal forces and the intensity in beams can be estimated as function of time. The individual components of intensity, which propagate in each direction, and the components due to shear and moment can also be estimated.

The estimates are obtained by digitally filtering and combining the outputs of an array of sensors. The appropriate FIR filters are designed in the frequency domain, the approach being based on wave decomposition.

A number of experiments have been performed in order to investigate the behaviour of flexural waves in a thin beam.



# TABLE OF CONTENTS

<b>ABSTRACT.</b>	ii
<b>TABLE OF CONTENTS.</b>	iii
<b>NOTATION.</b>	v
<b>LIST OF FIGURES.</b>	vii
<b>1- INTRODUCTION.</b>	1
<b>2- FLEXURAL WAVE MOTION IN BEAM STRUCTURES.</b>	
<b>2.1 Flexural Waves in Thin Beams.</b>	3
<i>2.1.1 Differential equation of motion.</i>	3
<i>2.1.2 Bending waves in beams.</i>	6
<b>2.2 Energy Flow in Beam Structures.</b>	7
<i>2.2.1 Structural intensity in beams.</i>	7
<i>2.2.2 Intensity components.</i>	7
<b>2.3 Reflection and Transmission of Flexural Waves in beams.</b>	8
<b>3- WAVE AMPLITUDE FILTERS.</b>	
<b>3.1 Fundamentals in Designing Wave Amplitude Filters.</b>	10
<i>3.1.1 Wave decomposition in the frequency domain.</i>	10
<i>3.1.2 Wave reconstruction in the time domain.</i>	12
<b>3.2 Designing the FIR Filters.</b>	13
<b>3.3 Real-Time Estimation of Flexural Waves.</b>	14
<i>3.3.1 Farfield estimation.</i>	14
<i>3.3.2 Nearfield estimation.</i>	16

## **4- EXPERIMENTAL WORK.**

<b>4.1 Estimating the Flexural Wavenumber (<math>k</math>).</b>	18
<b>4.2 Real-Time Estimation of the Flexural Wave Amplitudes.</b>	20
<i>4.2.1 Experimental set-up and procedure.</i>	20
<i>4.2.2 Calculating the optimum spacing between sensors.</i>	22
<i>4.2.3 Designing the wave amplitude filters using Matlab© facilities.</i>	23
<b>4.3 Reflection and Transmission Coefficients Due to Mass Discontinuity.</b>	26
<i>4.3.1 Theoretical wave reflection and transmission.</i>	26
<i>4.3.2 Estimating <math>r</math> and <math>t</math> in the frequency domain.</i>	28

## **5- RESULTS AND DISCUSSION.**

<b>5.1 Real-Time Comparison of the Estimated Wave Amplitudes.</b>	31
<i>5.1.1 Discrete frequency excitation.</i>	31
<i>5.1.2 Broadband excitation.</i>	34
<b>5.2 Investigating the Validity of the Theoretical Modelling of the Transmission Coefficient <math>t</math> Due to Mass Discontinuity.</b>	36

## **6- CONCLUSION AND DISCUSSION.**

<b>6.1 General Concluding Remarks.</b>	38
<b>6.2 Future Work.</b>	38



<b>APPENDICES.</b>	39
A1.0 The boundary conditions of the four common cases of beam ends.	40
A2.0 Experimental equipment.	41
A3.0 Simulink block diagram for the estimated wave amplitude of the 3 configurations.	43
A4.0 The Matlab M-files of the designed wave filters.	
<b>REFERENCES</b>	50



## NOTATION

The lower case variable represents a symbol (e.g.,  $p(t)$ ) is used to represent a variable in the time domain while in the upper case (e.g.,  $P(\omega)$ ), represents the same variable in the frequency domain.

$A$	Cross sectional area.
$a^+$	Positive – going propagating wave.
$a_N^+$	Positive – going evanescent wave.
$a^-$	Negative – going propagating wave.
$a_N^-$	Negative – going evanescent wave.
$b^+$	Positive – going transmitting wave.
$b_N^+$	Positive – going transmitting evanescent wave.
$e$	Base of natural logarithm.
$E$	Young's modulus.
$f$	Frequency.
$f_N$	Nyquist frequency.
$f_s$	Sampling frequency.
$h$	Filter impulse response, FIR filter coefficient.
$H$	Filter frequency response.
$i$	$\sqrt{-1}$ .
$I$	Second moment of area.
$k$	Bending wavenumber.
$\bar{k}_t$	Translational stiffness.
$L$	Length of beam.
$m$	Bending moment.
$n$	Time step.
$n_d$	Time delay.
$n_t$	Number of terms in FIR filter.
$q$	Shear force.
$r$	Reflection coefficient.

$t$	Transmission coefficient.
$v$	Velocity.
$w$	Transverse displacement.
$x$	Longitudinal displacement.
$Y$	Sensor output.
$\Delta$	Spacing between two accelerometers.
$\theta$	Beam rotation.
$\lambda$	Wavelength.
$\rho$	Density.
$\Phi^+$	Positive – going propagating wave (frequency domain).
$\Phi^-$	Negative – going propagating wave (frequency domain).
$\Phi_N^+$	Positive – going evanescent wave (frequency domain).
$\Phi_N^-$	Negative – going evanescent wave (frequency domain).
$\omega$	Circular frequency.
$\dot{(\ )}$	$d(\ )/dt$
$(\ )'$	$d(\ )/dx$

### **Subscripts**

$m$	Time step number.
$n$	Nyquist frequency.
$N$	Nearfield.
$s$	Sampling frequency.

## LIST OF FIGURES

- Figure 2.1 Beam in flexure; positive sign convention.
- Figure 2.2 Definition of the positive shear force and bending moment.
- Figure 2.3 Nearfield waves.
- Figure 2.4 Point supported beam.
- Figure 3.1 Nearfield wave amplitudes.  $A_n$  is the accelerometer at position  $n$ , where  $n = 1, 2$  and  $3$ .
- Figure 3.2 Beam structure comprising two accelerometers in the farfield for estimating wave amplitude and intensity at  $x = \Delta/2$ .
- Figure 4.1 The sensor arrangement used in estimating  $k$ .
- Figure 4.2 The measured value of  $\cos(k\Delta)$  and its best fit.  
 \_\_\_\_\_ measured; ..... best fit.
- Figure 4.3 Experimental configurations with locations of accelerometers and shaker indicated (all dimensions in  $m$ ).
- Figure 4.4 The general experimental set-up used in the 2<sup>nd</sup> configuration.
- Figure 4.5 Simulink blocks of the farfield array.
- Figure 4.6 Simulink blocks of the nearfield array.
- Figure 4.7 Simulink blocks for the Fir filters used to estimate the wave amplitudes of the nearfield array.
- Figure 4.8 Infinite beam with mass discontinuity.
- Figure 4.9 Transmission and reflection coefficients of flexural waves on an infinite Euler-Bernoulli beam with a mass discontinuity.  
 \_\_\_\_\_  $|t|$ ; .....  $|r|$ ; -----  $|r_N|$ .
- Figure 4.10 Beam structure comprising four accelerometers in two arrays.
- Figure 4.11 The experimental set-up used for estimating the propagating wave amplitudes (all dimensions in  $m$ ).
- Figure 5.1 The effect of changing  $n_d$  on estimating the wave amplitudes of the first configuration.  
 \_\_\_\_\_  $\phi^+$ ,  $n_d = 5$ ; .....  $\phi^+$ ,  $n_d = 15$ ;  
 -----  $\phi^-$ ,  $n_d = 5$ ; -.-.-  $\phi^-$ ,  $n_d = 15$ .

Figure 5.2 Comparison between the propagating waves estimated by both approaches for the first configuration.  $n_d = 5$ ,  $f = 100$  Hz.

——  $\phi^+$ , of farfield array; .....  $\phi^+$ , of nearfield array.  
 -----  $\phi^-$ , of farfield array; -.-.-  $\phi^-$ , of nearfield array.

Figure 5.3 The propagating waves of the first configuration,  $n_d = 5$ ,  $f = 100$  Hz.

——  $\phi^+$ ; -----  $\phi^-$ .

Figure 5.4 The flexural wave amplitudes estimated from both arrays of the second configuration,  $n_d = 5$ ,  $f = 100$  Hz.

- (a) Positive propagating waves: ——  $\phi^+$ , of farfield array; .....  $\phi^+$ , of nearfield array.  
 (b) Negative propagating waves: -----  $\phi^-$ , of farfield array; -----  $\phi^-$ , of nearfield array.  
 (c) Positive waves: ——  $\phi_N^+$ ; .....  $\phi^+$ , of nearfield array.

Figure 5.5 Spectral densities of the estimated wave amplitudes of the third configuration,  $n_d = 5$ :

- (a) Positive propagating waves: ——  $\phi^+$ , of farfield array; -----  $\phi^+$ , of nearfield array; .....  $\phi^-$ , of farfield array; -.-.-  $\phi^-$ , of nearfield array.  
 (b) Positive waves: ——  $\phi^-$ , of nearfield array; -----  $\phi_N^+$  (experimentally); .....  $\phi_N^+$  (Theoretically).

Figure 5.6 Comparison between the theoretical and experimental attenuation occurred to the incident wave due to mass discontinuity.

——  $|t|$  (Theoretical); -----  $|t|$  (Experimentally).

Figure 5.7 Comparison between the theoretical and experimental attenuation occurred to the incident wave. No mass is attached experimentally.  
 .....  $|t|$  (Theoretical estimation-mass attached); ----- (Experimental estimation).

Figure 5.8 Satisfying the conservation of energy  $|r|^2 + |t|^2 = 1$ .

- (a) Experimentally: —— no mass attached; —— mass us attached.  
 (b) Theoretically: -----

# 1. INTRODUCTION.

In this report, both incident and reflected waves were estimated plus a positive-going nearfield one in real-time. In previous work, only positive propagating wave was estimated in real-time and this was used as a cost function in a feedforward adaptive control scheme [1,2,3].

These estimated waves were found by digitally filtering and combining the output of an array of sensors. From these waves, instantaneous intensity can be estimated once estimates from the instantaneous velocity, shear force, angular velocity, and bending moment at a point have been made [4].

This method of estimating the wave amplitudes in real-time is very effective and the main prerequisite is a successful estimation of the flexural wave number of the beam structure. Thus it will be used in the designed wave filters as will be explained.

The new wave estimates will partly be used in further research concerns adaptive-passive control of structure-borne vibration as a cost function.

The validity of theoretical modelling of the reflection and transmission of flexural waves due to mass discontinuity [5] was investigated experimentally in the frequency domain. This is presented here as a basic experimental work for a potential application for real-time wave amplitude of more complicated discontinuity systems.

The report is presented in five main chapters; an introduction about flexural wave motion in beam structures is introduced in Chapter 2. Reflection and transmission of waves due to point discontinuities and boundary conditions are briefly introduced.

Chapter 3, "Wave Amplitude Filters," presents the major fundamentals in designing the wave amplitude filters. Wave decomposition and reconstruction method is introduced. The estimation of flexural waves in beam structures has been implemented in both far- and nearfield.

Chapter 4, "Experimental Work," presents the experimental set-up followed in the performed experiments. An explanation about the designed wave amplitude filters using the Matlab facilities is also included.

Chapter 5, "Experimental Results," presents a discussion about the experimental results performed.

A comparison between the estimated wave amplitudes has been shown for both discrete frequency and broadband excitation.

Moreover, the validity of theoretical modelling of transmission coefficient has been investigated.

Lastly, the most important remarks obtained from the experimental work as well as the future planned work were included in Chapter 6.



## **2. FLEXURAL WAVE MOTION IN BEAM STRUCTURES.**

This chapter introduce some back knowledge about flexural waves in Euler-Bernoulli beams and the effect of point discontinuities and boundary conditions on wave motion. The chapter is organised in three sections. The flexural wave motion in beams was introduced in the first section.

The second section explains the energy flow in beams. Effect of discontinuities and boundary conditions on the behaviour of flexural waves was briefly introduced in the third section.

### **2.1 Flexural Waves in Thin Beams.**

Vibrations propagate through structures as waves, where a mechanical wave may be defined as “a phenomenon in which a physical quantity (e.g., energy or strain) propagates in a supporting medium, without net transport of the medium.”[6]

When mass and elasticity are distributed through a system, a description of its configuration requires an infinite number of coordinates. Therefore beams have an infinite number of degrees of freedom, which in turn means that it has an infinite number of natural frequencies.

The vibrational behaviour of beams is of great interest to engineers, where it is found that their lower natural frequencies often have values, which give rise to the possibility of resonance occurring when machinery is running.

It is found that the flexural waves are the easiest to excite in beams structures, however axial and torsional vibrational motions are also possible to exist.

This displacement occurred to a beam element due to flexural vibration consists of four wave components as will be explained in this chapter.

#### **2.1.1 Differential equation of motion.**

Using the Bernoulli-Euler beam theory; namely that the beam is initially straight, and that the depth of the beam is small compared with its radius of curvature at its maximum displacement. In another way, plane sections remain plane and perpendicular to the neural axis of bending [6,7,8].

The sign convention adopted is shown in Figure 2.1 together with the forces and moments acting on an elemental length of the beam in its distorted form.

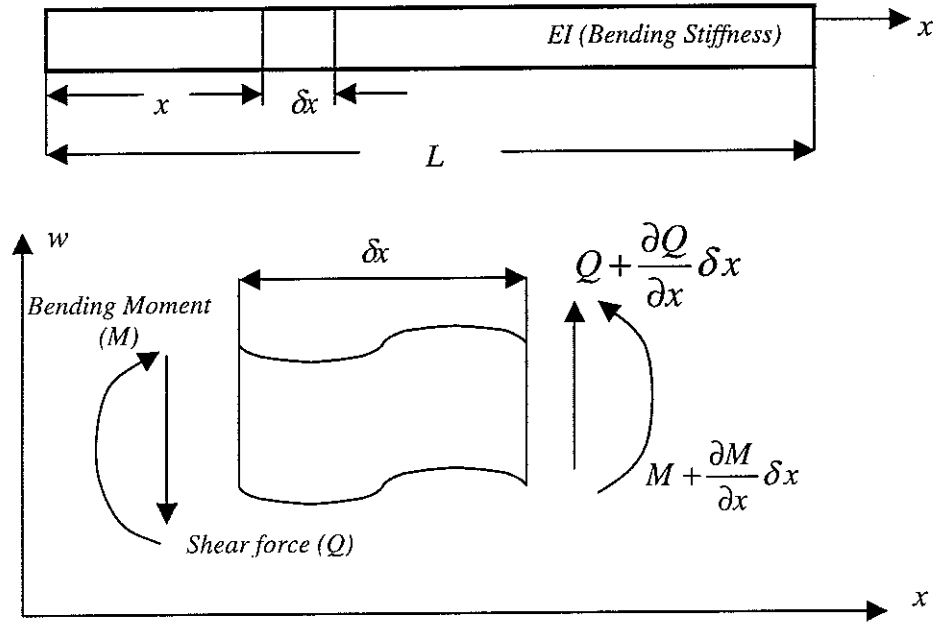


Figure 2.1. Beam in flexure; Positive sign convention

Applying Newton's laws gives for motion in the  $y$  direction

$$\frac{\partial Q}{\partial x} = \rho A \frac{\partial^2 w}{\partial t^2}. \quad (2.1)$$

By summing moments of the elemental length  $\delta x$ , it is found that

$$Q = -\frac{\partial M}{\partial x}, \quad (2.2)$$

using this value for  $Q$  in Equation (2.1) gives

$$\frac{\partial^2 M}{\partial x^2} + \rho A \frac{\partial^2 w}{\partial t^2} = 0. \quad (2.3)$$

Bernoulli – Euler beam theory gives the following relationships between the applied moment and the curvature.

$$M = EI \frac{\partial^2 w}{\partial x^2}, \quad (2.4)$$

and hence

$$Q = -EI \frac{\partial^3 w}{\partial x^3}, \quad (2.5)$$

where the direction of the positive shear force and bending moment is shown in Figure 2.2.

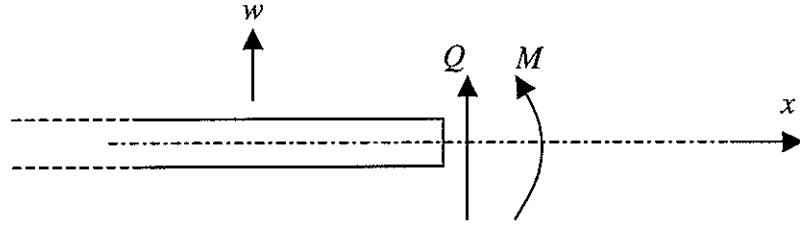


Figure 2.2. Definition of the positive shear force and bending moment

Therefore the equation of motion is

$$EI \frac{\partial^4 w}{\partial x^4} + \rho A \frac{\partial^2 w}{\partial t^2} = 0. \quad (2.6)$$

For simple harmonic motion  $w(x,t) = W(x)e^{i\omega t}$

$$\therefore EI \frac{d^4 W}{dx^4} - \rho A \omega^2 W = 0. \quad (2.7)$$

The general solution to this equation is the sum of four harmonics as shown below

$$W(x) = A \sin kx + B \cos kx + C \sinh kx + D \cosh kx,$$

where  $W$  is the beam's displacement.  $A$ ,  $B$ ,  $C$  and  $D$  are arbitrary constants and the frequency dependent variable  $k$  is given below

$$k = \sqrt[4]{\frac{\rho A}{EI}} \sqrt{\omega}, \quad (2.8)$$

which is the flexural wavenumber. This gives phase change per unit distance that describes the spatial variations [9]. The constants  $\rho$ ,  $A$ ,  $E$ , and  $I$  represents the beam's density, cross sectional area, Young's Modulus and the second moment of are respectively. The variable  $\omega$  represents the circular frequency. The relation between the wavenumber  $k$  and wavelength  $\lambda$  is given by

$$k = \frac{\omega}{c_B} = \frac{2\pi}{\lambda}, \quad (2.9)$$

where  $c_B$  is the speed at which the disturbance propagate in a system and it is called the phase velocity.

One of the unique characteristics of flexural waves is the dispersion property, where the phase velocity  $c_B$  increases without limit for increasing wavenumber  $k$  for shorter wavelength  $\lambda$ .

### 2.1.2 Bending waves in beams.

Suppose quantities vary time harmonically at a frequency  $\omega$ . Hence eq.(2.7) becomes

$$\frac{d^4 W}{dx^4} - k^4 W = 0. \quad (2.10)$$

The general solution of Eq.(2.10) including the time dependence term  $e^{i\omega t}$  is given by

$$w(x, t) = a^+ e^{i(\omega t - kx)} + a^- e^{i(\omega t + kx)} + a_N^+ e^{i\omega t} e^{-kx} + a_N^- e^{i\omega t} e^{kx}, \quad (2.11)$$

where  $a^+ e^{i(\omega t - kx)}$  and  $a^- e^{i(\omega t + kx)}$  represent positive and negative going waves respectively, while  $C e^{i\omega t} e^{-kx}$  and  $D e^{i\omega t} e^{kx}$  represent positive and negative decaying evanescent waves respectively.

Nearfield, or evanescent waves, are waves that decay exponentially with distance. These are very localised and usually do not carry energy. The exponential decaying of these waves is shown in Figure 2.2.

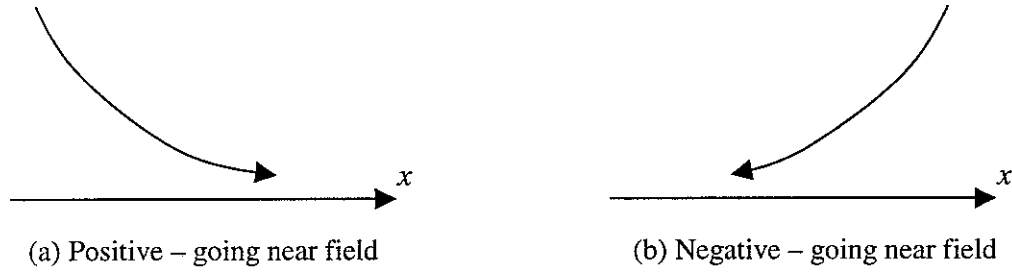


Figure 2.3. Near field waves

Hereafter, the explicit time dependence  $e^{i\omega t}$  will be suppressed; hence the beam displacement  $w$  given in Eq.(2.11) can be reduced to the one below in the frequency domain

$$W(x, \omega) = \Phi_w^+ e^{-ikx} + \Phi_{w,N}^+ e^{-ikx} + \Phi_w^- e^{+ikx} + \Phi_{w,N}^- e^{+ikx}. \quad (2.12)$$

In the presence of damping,  $k$  has negative (usually small) imaginary part so that the amplitude of the propagating wave component decays gradually in the direction of propagation.

The wave amplitudes  $\Phi_w$  are thus referred to as displacement wave amplitude. The subscript  $N$  refers to the evanescent waves. However, all response quantities (velocity, acceleration, shear force, etc...) vary time harmonically under the passage of a wave.

Thus, it is possible to define the amplitudes of the wave components in terms of the amplitude of any such response quantity. For example, velocity waves, which have amplitudes  $\Phi_v = i\omega\Phi_w$ , give the velocity of a beam under the passage of a wave while acceleration waves have amplitudes  $\Phi_A = -\omega^2\Phi_w$ .

The superposition of these waves gives the velocity or acceleration of the wave-guide.

## 2.2 Energy Flow in Beam Structures.

This section presents the energy flow in beams structures and intensity components in terms of the flexural wave amplitudes.

### 2.2.1 Structural intensity in beams.

The flow of vibrational energy along the beam structure is called the structural intensity and this is given in terms of beam deformation and internal forces by

$$i(x,t) = -qv - m\dot{\theta}; \quad v = \frac{\partial w}{\partial t}; \quad \dot{\theta} = \frac{\partial^2 w}{\partial x \partial t}, \quad (2.13)$$

where  $v$  and  $\dot{\theta}$  are the transverse and rotational velocities respectively.

The total intensity in the beam arises from three terms [4,10]. The two propagating waves independently, where each wave has shear and moment contributions to the total intensity, which are equal in magnitude and out of phase, so that their sum is constant and independent of time. The nearfield interaction terms, however, give a contribution, that depends on the relative phases of the wave components.

### 2.2.2 Intensity components.

Measuring the internal forces in practice is very difficult. The beam response is instead measured at a number of points and the internal forces are then inferred from equations (2.4) and (2.5) as shown using the finite difference approach by Pavic [11]. The intensity can be estimated directly if the velocities and internal forces are known [4,5]. The internal forces and the rotational velocity can be estimated by using a wave decomposition approach.

One can find the structural intensity in the frequency domain by deriving the intensity components as shown below

$$\begin{aligned} \begin{Bmatrix} W \\ (1/k\omega)\dot{\theta} \end{Bmatrix} &= \begin{bmatrix} e^{-ikx} & e^{-kx} \\ e^{-ikx} & -ie^{-kx} \end{bmatrix} \begin{Bmatrix} \Phi_w^+ \\ \Phi_{w,N}^+ \end{Bmatrix} + \begin{bmatrix} e^{ikx} & e^{kx} \\ -e^{ikx} & ie^{kx} \end{bmatrix} \begin{Bmatrix} \Phi_w^- \\ \Phi_{w,N}^- \end{Bmatrix}, \\ \begin{Bmatrix} M/EIk^2 \\ Q/EIk^3 \end{Bmatrix} &= \begin{bmatrix} -e^{-ikx} & e^{-kx} \\ -ie^{-ikx} & e^{-kx} \end{bmatrix} \begin{Bmatrix} \Phi_w^+ \\ \Phi_{w,N}^+ \end{Bmatrix} + \begin{bmatrix} -e^{ikx} & e^{kx} \\ ie^{ikx} & e^{kx} \end{bmatrix} \begin{Bmatrix} \Phi_w^- \\ \Phi_{w,N}^- \end{Bmatrix}. \end{aligned} \quad (2.14)$$

Therefore, shear and moment contributions of the intensity can be deduced respectively below in the time domain

$$-q(t)v(t) = -\text{Re}\{Q(\omega)e^{i\omega t}\}\text{Re}\{\dot{W}(x)e^{i\omega t}\}, \quad (2.15)$$

and

$$-m(t)\dot{\theta}(t) = -\text{Re}\{M(\omega)e^{i\omega t}\}\text{Re}\{(\dot{W}(x))'e^{i\omega t}\}. \quad (2.16)$$

Summing equations (2.15) and (2.16) will lead to the total intensity.

### 2.3 Reflection and Transmission of Flexural Waves in Beams.

This section will present a brief introduction about the effect of discontinuities and boundary conditions on the flexural waves along beam structures. The transmission of the flexural waves can be suppressed if the point discontinuity is well designed.

Suppose a positive – going wave  $\Phi^+$  is incident upon a support as shown in Figure 2.3. It gives rise to positive-going transmitted  $\Phi_T^+$  and negative-going reflected  $\Phi^-$  waves

$$\frac{\Phi^-}{\Phi^+} = r; \frac{\Phi_T^+}{\Phi^+} = t, \quad (2.17)$$

where  $r$  and  $t$  are the reflection and transmission coefficients respectively.

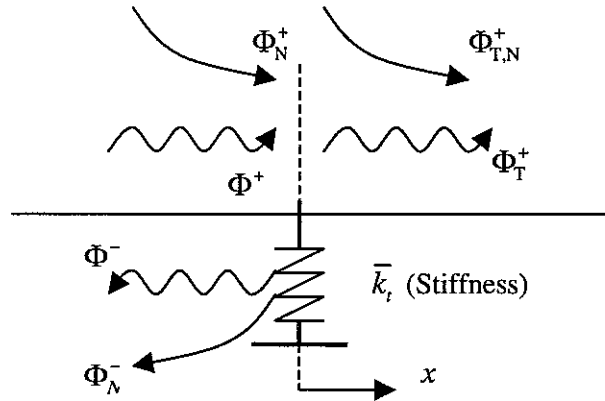


Figure 2.4. Point supported beam.

The displacements of the beam  $w_-$  and  $w_+$  in the regions  $x \leq 0$  and  $x \geq 0$  are given by:

$$W_- = \Phi_w^+ e^{-ikx} + \Phi_{w,N}^+ e^{-ikx} + \Phi_w^- e^{+ikx} + \Phi_{w,N}^- e^{+ikx}, \quad W_+ = \Phi_T^+ e^{-ikx} + \Phi_{T,N}^+ e^{-ikx}. \quad (2.18)$$

The amount of transmitted wave depends on the characteristics of the point discontinuity as shown by Hassan [10].

There are two conditions that can be satisfied at each end of the beam. The four most commonly cases of boundary conditions are listed in Appendix A1.0.

### 3. WAVE AMPLITUDE FILTERS

This chapter presents the algorithm of the wave amplitude filters used in estimating the flexural wave amplitudes. It is organised in five sections, where the first one introduces the important fundamentals in designing the wave amplitude filters. A brief discussion about the methods of designing the FIR filters and the factors controlling their accuracy over the frequency range of interest is presented in second section. The third section concerns with estimating the ideal frequency responses of the digital filters. These were used to estimate the propagating wave amplitudes of the farfield where the evanescent waves are insignificant and this will require designing four digital filters. The ideal frequency responses used in estimating the nearfield wave amplitudes (two propagating waves plus the positive decaying nearfield) are also included.

#### 3.1 Fundamentals in Designing Wave Amplitude Filters.

This section presents some basic knowledge about designing the wave amplitude filters using the wave decomposition and reconstruction approach as explained by Mace [4,12]. The filters are designed in the frequency domain and subsequently implemented in the time domain by convolving the sensor outputs with the impulse responses of various filters. A brief discussion about the ideal frequency responses used in these filters is also included.

##### 3.1.1 Wave decomposition in the frequency domain.

An array of three equally spaced sensors are mounted on a beam is shown in Figure 3.1. The output of the sensors are digitally filtered and combined to yield estimates of the wave amplitudes at the centre of the array  $x = 0$ . These filters are referred to as wave filters or wave amplitude filters.

It is assumed that the negative going nearfield  $\Phi_N^-$  is negligible, although its effects are included in the simulations as described later. The displacement around the array can be written as

$$W(x, \omega) = \Phi^+ e^{-ikx} + \Phi_N^+ e^{-kx} + \Phi^- e^{ikx}. \quad (3.1)$$

The subscript  $W$ , which referred to displacement wave amplitudes, is omitted for simplicity.



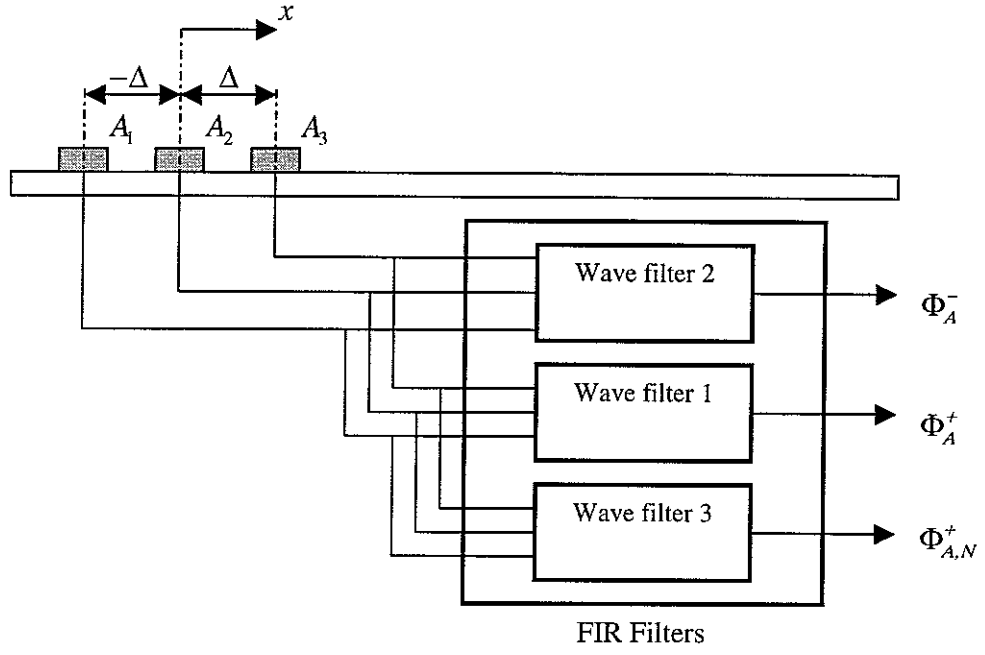


Figure 3.1. Nearfield wave amplitudes.  $A_n$  is the accelerometer at position  $n$ , where  $n=1,2$  and  $3$ .

The vector of sensor outputs  $\mathbf{Y}(\omega)$  is related to the wave amplitudes  $\Phi(\omega)$  by

$$\mathbf{Y}(\omega) = \begin{Bmatrix} W(-\Delta, \omega) \\ W(0, \omega) \\ W(\Delta, \omega) \end{Bmatrix}, \quad (3.1)$$

and hence

$$\mathbf{Y}(\omega) = \mathbf{S}(\omega) \Phi(\omega); \quad \Phi(\omega) = \begin{Bmatrix} \Phi^+ \\ \Phi^- \\ \Phi_N^+ \end{Bmatrix}, \quad (3.2)$$

where the sensor matrix

$$\mathbf{S}(\omega) = \begin{bmatrix} e^{ik\Delta} & e^{-ik\Delta} & e^{k\Delta} \\ 1 & 1 & 1 \\ e^{-ik\Delta} & e^{ik\Delta} & e^{-k\Delta} \end{bmatrix}. \quad (3.3)$$

The wave amplitudes are consequently given by

$$\Phi(\omega) = \mathbf{G}(\omega)\mathbf{Y}(\omega); \mathbf{G}(\omega) = \mathbf{S}^{-1}(\omega). \quad (3.4)$$

Thus, the frequency response matrix  $\mathbf{G}(\omega)$  can be found by inverting  $\mathbf{S}(\omega)$ . This can be easily calculated using software such as Matlab®.

The determinant of  $\mathbf{S}$  equals  $4i \sin ka (\cosh ka - \cos ka)$ , and hence  $\mathbf{S}$  is singular if the separation  $\Delta$  is half a wavelength  $(\lambda/2)$ .

The matrix  $\mathbf{G}(\omega)$  provides wave amplitudes of the same response variable as the sensor outputs, i.e. accelerations measurements would give acceleration wave amplitudes as shown in Figure 3.1. Therefore  $-1/\omega^2 \mathbf{G}$ , and  $1/i\omega \mathbf{G}$  would provide estimates of displacement- and velocity-wave amplitudes respectively.

### 3.1.2 Wave reconstruction in the time domain.

The wave amplitude is given by the superposition of the related frequency components. Where

$$\phi(t) = F^{-1}\{\Phi(\omega)\} = \int_{-\infty}^{\infty} \Phi(\omega) e^{i\omega t} d\omega \quad (3.5)$$

where  $F^{-1}\{.\}$  is the inverse Fourier transform. Therefore the wave amplitudes in real-time  $\phi$  can be found below

$$\phi(t) = \mathbf{g}(t) * \mathbf{y}(t), \quad (3.6)$$

where  $*$  denotes the convolution and  $\mathbf{g}(t)$  is a matrix of impulse responses, these are the inverse Fourier transforms of the elements of  $\mathbf{G}(\omega)$ . These will be explained later on in the experimental work. Where the steps in implementing the wave filters are thus to specify the details of the sensor array to determine the frequency response matrix  $\mathbf{G}(\omega)$ , and to design filters whose impulse response approximate  $\mathbf{g}(t)$  to acceptable accuracy. This will involve the implementation of Finite Impulse Response (**FIR**) digital filters.

The required filters are typically non-causal, so that  $\mathbf{g}(t)$  is non-zero for  $t < 0$ . as a result of estimating the wave amplitude at  $x=0$  from sensor measurements at various locations. Also it takes some time for waves to propagate from one location to another. Therefore exact estimation of the wave amplitudes requires knowledge of the

future output of the downstream sensor. These effects can be minimized by incorporating small delay into the filtering process\*.

### 3.2 Designing the FIR Filters.

All filtering is performed digitally, with the accelerations assumed to be sampled at a sampling frequency  $f_s$ , being first passed through anti – aliasing low-pass filters with a cut-off frequency of somewhat less than the Nyquist frequency  $f_n = f_s / 2$ .

The estimated wave amplitude at time step  $m$  is then

$$\phi_m = \sum_{i=1,3} \left( \sum_{p=0,P} g_p y_{j,m-p} \right) \quad (3.7)$$

where the length of the filters is  $P+1$ . The implemented filters are consequently approximations to the ideals defined above. There are a number of ways of designing FIR filters. The adopted approach is the one described by Mace [1].

The filters in  $\mathbf{G}$  are time delayed by  $n_d$  time step, which is equivalent to multiplying  $\mathbf{G}$  by  $\exp(-i\omega n_d / f_s)$ . Therefore the number of terms in the FIR filter  $n_t$  can be found below

$$n_t = (2n_d + 1). \quad (3.8)$$

The FIR filters are only accurate over a frequency range, which is limited by a number of factors [1]:

- 1- The selected sampling frequency  $f_s$  (Max. frequency of control being less than the Nyquist frequency).
- 2- The sensor spacing  $\Delta$  must be less than half the wavelength for a given frequency range.
- 3- The lower frequency limits is imposed that the array should be free of the influence of the near field of the control.

FIR filters are insensitive to frequencies below  $\cong f_n / n_t$  and above  $f_n(1 - 1/n_t)$ .

A weighed least-squares procedure is then used to fit the implemented frequency response  $\hat{\mathbf{G}}$  to that of the appropriate element of  $\mathbf{G}$ . This will minimize the sum over frequency of  $\left( \sigma(\omega) |G(\omega) - \hat{G}(\omega)|^2 \right)$ , where  $\sigma(\omega)$  is a chosen weight function.

The accuracy of the implemented filters depends on the number of terms and is generally worst for low frequencies and for frequencies close to the Nyquist

frequency  $f_N$ . these frequency ranges can be zero-weighted by in the least squares estimation if required.

In practise, the anti-aliasing filters will remove the low and high frequency components of the signals.

### 3.3 Real-Time Estimation of Flexural Waves.

This section presents the designed frequency responses of the wave filters. These concern the estimation of flexural waves in the Farfield and Nearfield of a thin beam.

#### 3.3.1 Farfield Estimation.

In the farfield, only propagating waves exist; hence an array of two accelerometers can be used to estimate the wave amplitude in real-time, where the accelerometer outputs are filtered using the digital FIR filters explained above.

Figure 3.2 shows a system comprising two accelerometers at distance  $\Delta$  apart, which is perhaps the most common system for estimating the structural intensity [4].

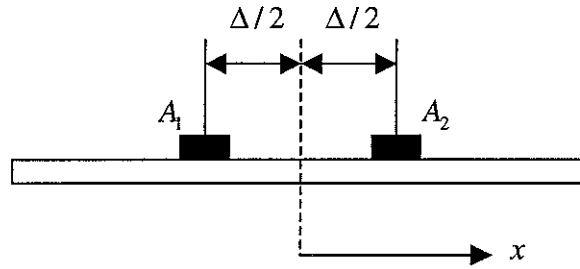


Figure 3.2. Beam structure comprising two accelerometers in the farfield for estimating wave amplitude and intensity at  $x = \Delta/2$

The two acceleration signals are digitally filtered in order to estimates the acceleration wave amplitudes.

The frequency responses  $H_1(\omega)$  and  $H_2(\omega)$  of the ideal filters are given by Mace [4], such that

$$\Phi_A^+ = H_1(\omega)(A_1(\omega) + A_2(\omega)) - H_2(\omega)(A_1(\omega) - A_2(\omega)), \quad (3.9)$$

$$\Phi_A^- = H_1(\omega)(A_1(\omega) + A_2(\omega)) + H_2(\omega)(A_1(\omega) - A_2(\omega)), \quad (3.10)$$

$$H_1^A = \frac{1}{4\cos(k\Delta/2)}, H_2^A = \frac{i}{4\sin(k\Delta/2)}, \quad (3.11)$$

where  $A_1$  and  $A_2$  are the accelerometer outputs at point 1 and 2 respectively, as shown in Figure 3.2.

The structural intensity can be estimated in real-time, by deducing the ideal frequency responses of the internal forces (shear force, bending moment, velocity and angular velocity). This can be written in wave components [1].

The displacement in the farfield of a beam can be written as

$$W = \Phi_w^+ e^{-ikx} + \Phi_w^- e^{ikx}. \quad (3.12)$$

The designed frequency responses of the intensity components are found below by employing equations (2.4), (2.5), and (2.13). Acceleration wave amplitudes were used for practical implementations as will be explained in the next chapter.

(1) Shear force ( $Q$ ):

$$Q^A = \frac{iEk^3}{\omega^2} (\Phi_A^+ - \Phi_A^-), \quad (3.13)$$

The ideal frequency response of shear force ( $HQ$ ) is given by  $HQ = iEk^3 / \omega^2$ .

(2) Bending moment ( $M$ ):

$$M^A = \frac{Ek^2}{\omega^2} (\Phi_A^+ + \Phi_A^-), \quad (3.14)$$

The ideal frequency response of the bending moment ( $HM$ ) is given by  $HM = Ek^2 / \omega^2$ .

(3) Transverse velocity ( $v$ ):

$$v^A = -\frac{i}{\omega} (\Phi_A^+ + \Phi_A^-), \quad (3.15)$$

The ideal frequency response of the transverse velocity ( $HV$ ) is given by  $HV = -i / \omega$ .

(4) Angular velocity ( $\dot{\theta}$ ):

$$\dot{\theta}^A = \frac{k}{\omega} (-\Phi_A^+ + \Phi_A^-), \quad (3.16)$$

Finally, the ideal frequency response of the angular velocity ( $HS$ ) is given by  $k / \omega$ .

Matlab© can be used in designing the FIR filters, using the ideal frequency responses found above. These estimated intensity components would lead to estimating the structural intensity.

---

\*The time delay will have profound consequences for applications such as active control.

### 3.3.2 Nearfield estimation.

Three signals are needed here, where a single evanescent wave exist (the negative-decaying evanescent waves is assumed to be insignificant). Hence one more accelerometer is required to estimate the positive-decaying nearfield ( $\Phi_N^+$ ) [12].

Sensors spacing were updated, in order that, the spacing between the outer sensors must be less than half the wavelength as will be explained in the next chapter.

The wave amplitudes can be found below by updating Eq.(3.4) to include the single evanescent wave

$$\begin{Bmatrix} \Phi^+ \\ \Phi^- \\ \Phi_N \end{Bmatrix} = \begin{bmatrix} G_{11} & G_{12} & G_{13} \\ G_{21} & G_{22} & G_{23} \\ G_{31} & G_{32} & G_{33} \end{bmatrix} \begin{Bmatrix} A_1 \\ A_2 \\ A_3 \end{Bmatrix}, \quad (3.17)$$

where  $A_1$ ,  $A_2$  and  $A_3$  are the point accelerations measured from the sensor array shown in Figure 3.1.

Similarly as the farfield case, the ideal frequency responses of the intensity components are given below. These will be used in the FIR filters.

(1) Shear force ( $Q$ ):

$$Q^A = \frac{EIk^3}{\omega^2} (i\Phi_A^+ - i\Phi_A^- - \Phi_N^+), \quad (3.18)$$

Two ideal frequency responses were implemented here due to the imaginary part ( $i$ ).

( $HQ1$ ) is given by  $HQ1 = iEIk^3 / \omega^2$ , and  $HQ2 = -EIk^3 / \omega^2$ .

(2) Bending moment ( $M$ ):

$$M^A = \frac{-EIk^2}{\omega^2} (-\Phi_A^+ - \Phi_A^- + \Phi_N^+), \quad (3.19)$$

The ideal frequency response of the bending moment ( $HM1$ ) is given by

$HM1 = -EIk^2 / \omega^2$ .

(3) Transverse velocity ( $v$ ):

$$v^A = \frac{-i}{\omega} (\Phi_A^+ + \Phi_A^- + \Phi_{A,N}^+), \quad (3.20)$$

The ideal frequency response of the transverse velocity ( $HV1$ ) is given by

$HV1 = -i / \omega$ .

(4) Angular velocity ( $\dot{\theta}$ ):

$$\dot{\theta}^A = \frac{k}{\omega}(-\Phi_A^+ + \Phi_A^- + i\Phi_{A,N}^+), \quad (3.21)$$

Two ideal frequency responses were implemented.  $HS1 = k / \omega$ , and  $HS2 = ik / \omega$ .

These ideal frequency responses will be used in the appropriate FIR filters as will be discussed in the next chapter.

## 4- EXPERIMENTAL WORK.

This chapter presents the experimental work carried out on an Euler-Bernoulli beam in three sections.

The flexural wavenumber ( $k$ ) of the beam was estimated as a function of frequency. This is described in the first section. The second section uses the wavenumber estimated in section one in the designed FIR filters, in order to estimate the flexural wave amplitude. This has been done for three distinct system configurations. A schematic design of the various wave amplitude filters are also include in this section. The third section includes a brief experimental work concerns the reflection and transmission of flexural waves due to mass discontinuity.

### 4.1 Estimating the Flexural wavenumber ( $k$ ).

The wavenumber ( $k$ ) of the beam is function of its properties and the frequency ( $f$ ), as given in Eq.(2.8).

Three accelerometers and an FFT analyser (HP3566A) were used in measure the acceleration at 3 positions on a thin beam over a frequency span of 0-1600Hz.

The spacing between sensors  $\Delta = 0.52m$  as shown in Figure 4.1.

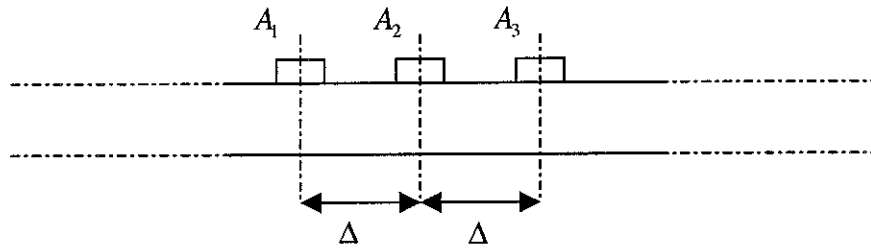


Figure 4.1. The sensor arrangement used in estimating  $k$ .

The accelerations estimated at the three sensor positions shown in Figure 1 can be written as function of the positive and negative propagating wave amplitudes [4] assuming that no nearfields are present, and are given by

$$\begin{aligned} A_1 &= \phi^+ e^{ik\Delta} + \phi^- e^{-ik\Delta} \\ A_2 &= \phi^+ + \phi^- \\ A_3 &= \phi^+ e^{-ik\Delta} + \phi^- e^{ik\Delta} \end{aligned} \quad , \quad (4.1)$$



where  $\phi^+$  and  $\phi^-$  represents the amplitudes of the positive and negative propagating waves. By summing  $A_1$  and  $A_3$ , then the following relation can be obtained.

$$\cos(k\Delta) = 0.5 \left( \frac{A_1}{A_2} + \frac{A_3}{A_2} \right). \quad (4.2)$$

Figure 4.2 shows the measured value of  $\cos(k\Delta)$  as function of frequency together with the best fit, which was found to be so when  $\beta = 0.8269$ . Therefore the estimated wavenumber ( $k$ ) as a function of frequency is

$$k = 0.8269\sqrt{f} \quad (4.3)$$

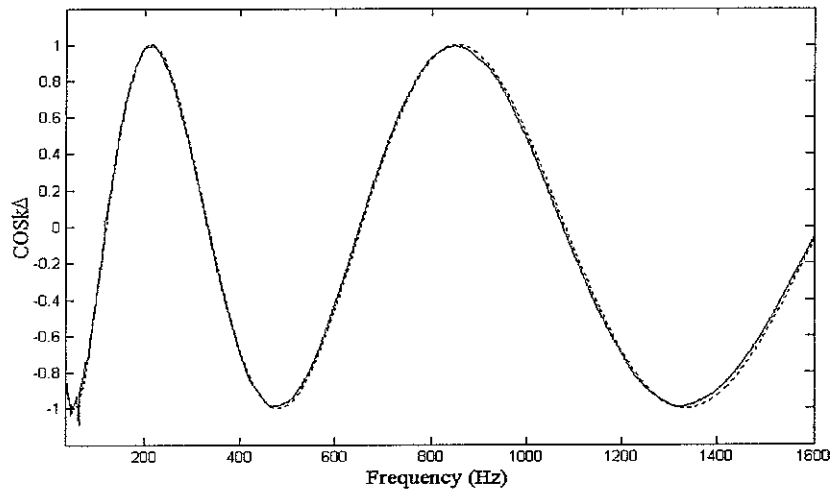


Figure 4.2. The measured value of  $\cos(k\Delta)$  and its best fit.

————— measured; .....best fit.

The difference between the new estimated wavenumber ( $k$ ) and the previous estimate (the one used in the first report) is 4.4%. This new estimated wavenumber has been used in updating the wave filters, which have been used in re-estimating the flexural wave amplitudes in the next section.

## 4.2 Estimating the Flexural Wave Amplitudes.

This section describes the experimental work carried out in order to estimate the flexural wave amplitudes. The wave amplitude filters are designed using the Matlab© facility.

### 4.2.1 Experimental set-up and procedure.

The experimental set-up comprised a steel beam of dimensions  $50.6 \times 6.4 \times 5630 \text{ mm}$  suspended at four points along its length. Brief description of the equipment used in the experiments is shown in Appendix A2.0.

The sampling rate ( $f_s$ ) implemented in the experiments was 1024Hz. FIR filters were designed with zero weighting being applied apart from the frequency range from  $0.1f_n$  to  $0.9f_n$ , where  $f_n$  is the Nyquist frequency ( $f_n = f_s/2$ ).

Three system configurations shown in Figure 4.3 are designed for various aims. The first system shown in Figure 4.3 (a) the 3 – sensor array is located in the farfield. It is used to compare the propagating wave amplitudes estimated from both farfield and nearfield approaches\* in the farfield. Thus the single evanescent wave  $\phi_N^+$  estimated from the nearfield approach was insignificant.

The aim of the second configuration shown in Figure 4.3 (b) was to compare the amplitudes of the propagating waves estimated from both approaches. The 3 – accelerometer approach is located in the nearfield of the force while the 2 – accelerometers approach is located in the farfield. In general, the negative propagating waves  $\phi^-$  should be small compared to the positive ones  $\phi^+$ .

---

\* The sensor array of the farfield approach includes 2 accelerometers, while the one of the nearfield approach includes 3 accelerometers. The latter approach is able to estimate a single evanescent wave while the farfield approach ignores the evanescent wave

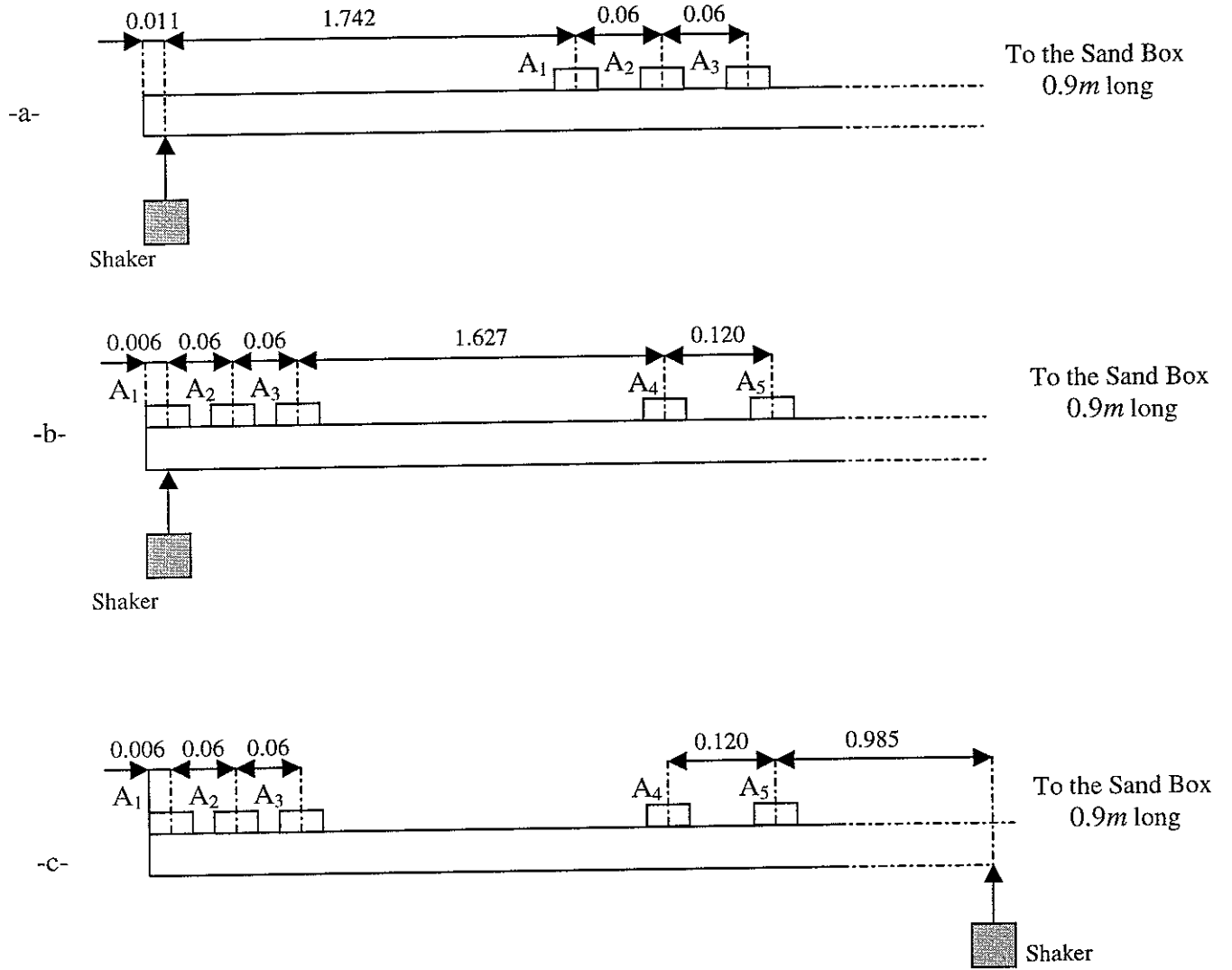


Figure 4.3. Experimental configurations with locations of accelerometers and shaker indicated (all dimensions in  $m$ ).

The measured wavenumber of the beam was such that  $k = 0.8269\sqrt{f}$ . It is very difficult to compare the wave amplitudes in the time domain, since no reference measurements can be made. Furthermore, the two signals were contaminated by errors introduced by the poor approximation of the filters at low and high frequencies. Therefore, the power spectral density (PSD) was used in the comparison.

The equipment used in each configuration was the same in all cases except that one more sensors were used in configuration b and c in figure 4.3. Figure 4.4 illustrates the general experimental set up.

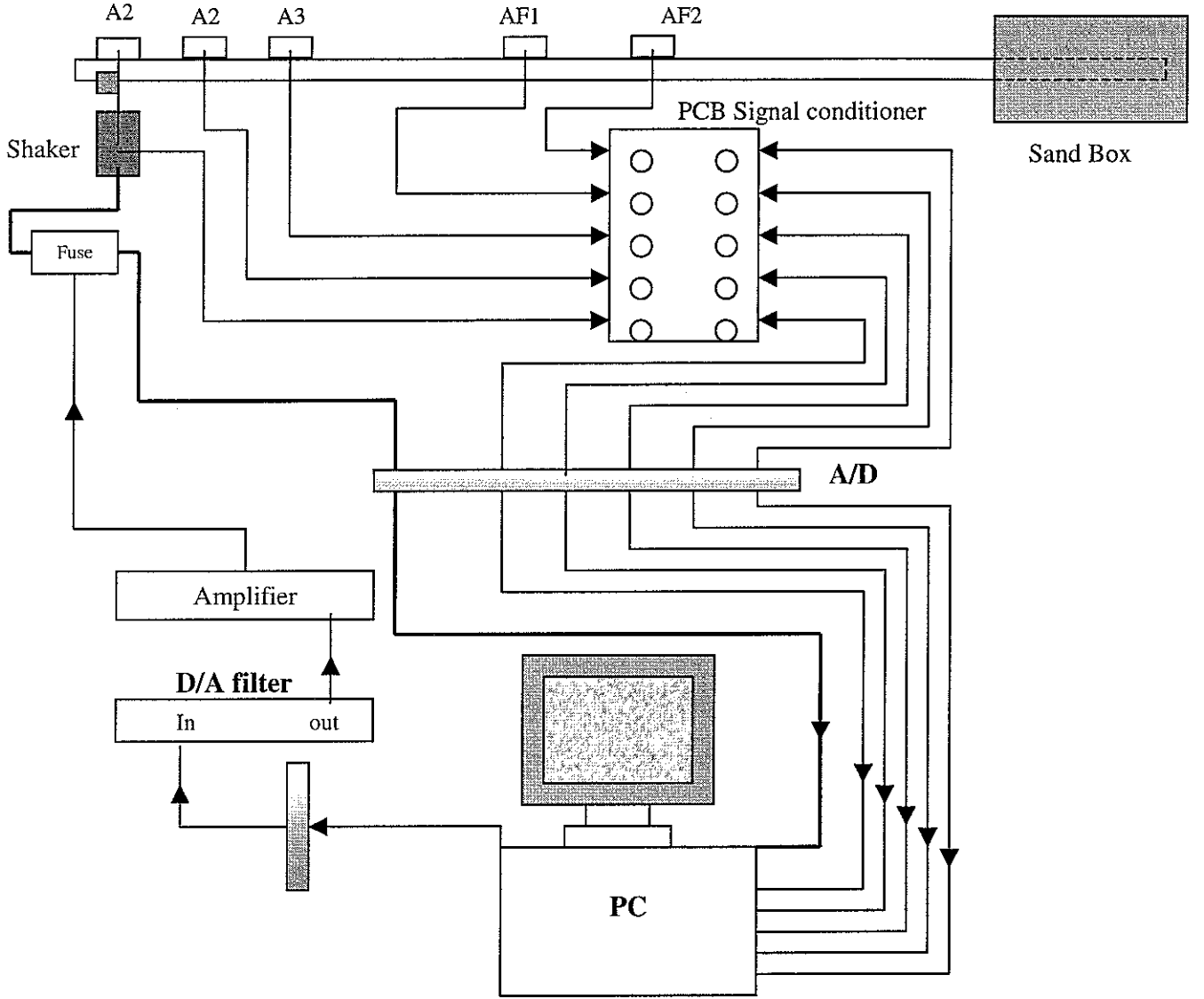


Figure 4.4. The general experimental set up used in the 2<sup>nd</sup> configuration.

#### 4.2.2 Calculating the optimum spacing between sensors.

As explained in section (3.3), the ideal frequency response in the farfield is

$$H_1 = \frac{1}{4 \cos(k\Delta/2)},$$

hence it is necessary that  $\frac{k\Delta}{2} < \frac{\pi}{2}$ . Therefore  $\Delta < \frac{\lambda}{2}$  [1], otherwise  $H_1$  will become infinite.

The minimum wavelength  $\lambda_{\min}$  for the maximum frequency employed (Nyquist frequency  $f_N$ ) is  $\lambda_{\min} = 0.3358m$ .

Therefore the maximum allowed spacing between the sensors should not exceed  $0.1679m$ . The implemented spacing was well below the limited as seen in Figure 4.3.

#### 4.2.3 Designing the wave amplitude filters using Matlab facilities.

The disturbance and control signals were generated by Pentium III 1 GHz PC (incorporating 256 Mb of RAM), equipped with a National Instruments PCI-MIO-16E-4, A-D/D-A board. All real-time processing was performed using Matlab and Simulink software incorporating the Real-Time Workshop and the **Real Times Windows Target (RTWT)**. The Simulink block diagrams are described below, where full models are given in Appendix A3.0 and the required Matlab M-Files are given in Appendix A4.0

The main parameters used in the experimental measurements are listed in Table 4.1

Sample Rate	1024 Hz
Wave number / Frequency relation	$k = 0.8269\sqrt{f}$
Frequency range	$0.2f_n - 0.8f_n$
Reconstruction filter, cut-off	350 Hz

Table 4.1 Parameters used in the experimental measurements.

Initial parameters were set or calculated using the M-Files **wave.m** and **Near.m**. These initial parameters include the wave number and the frequency relationship of the beam. The design of the band-pass filters are also included.

The M-Files used to design these filters are **coeff.m** for the farfield filters and **NearCoeffs.m** for the nearfield filters. All M-Files are located in Appendix D.

Two main roots were drawn in each Simulink model described in Appendix C. These are explained below

- 1- Estimating the propagating wave amplitudes of the farfield array. Four filters were used in order to estimate the positive and negative propagating wave amplitudes from two measured accelerations as shown in Figure 4.5. The blocks 'Wave filter' and 'Wave filter 4' were designed in this loop according to Equation (3.9) and Equation (3.11).

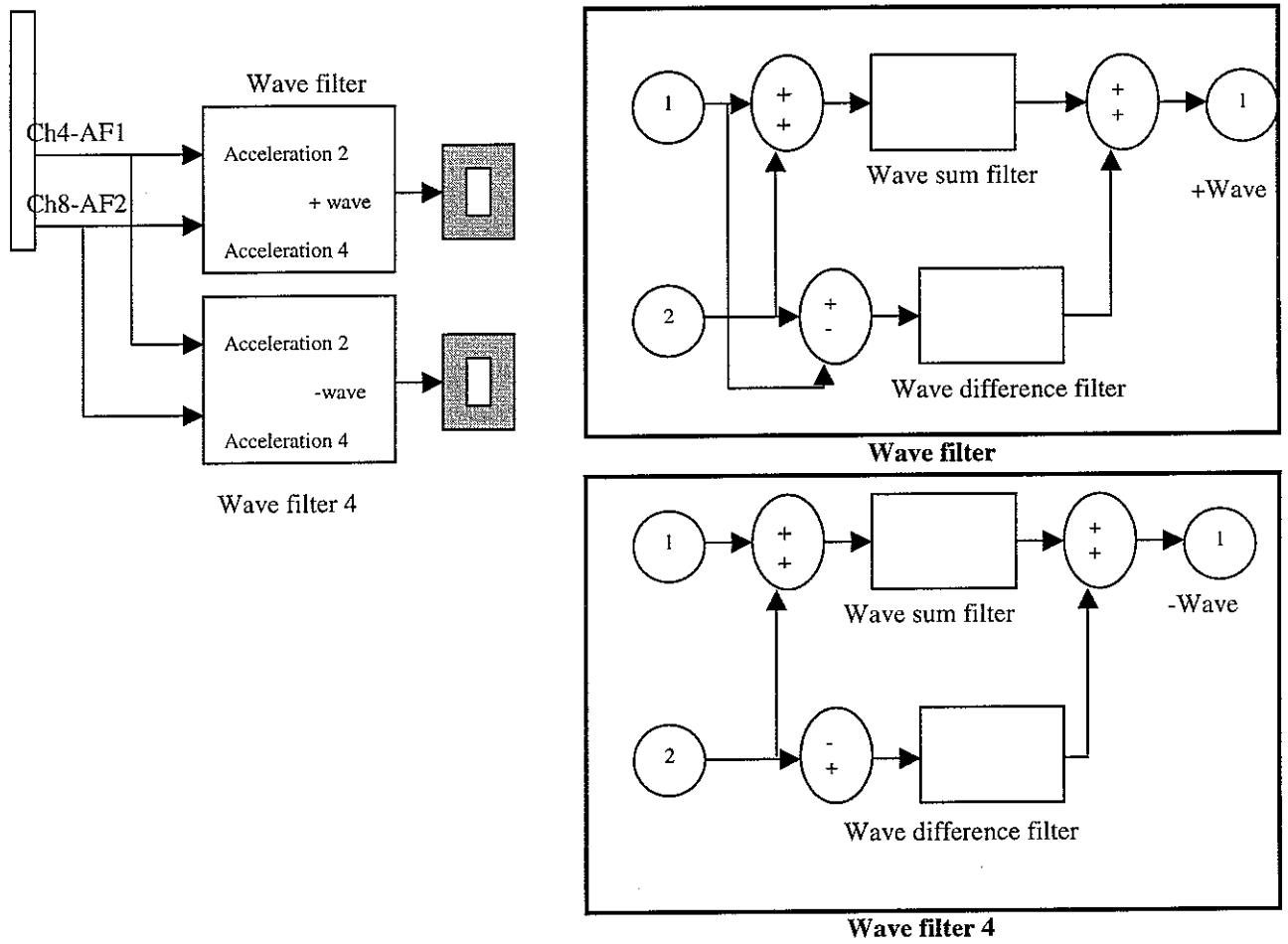


Figure 4.5. Simulink blocks of the Farfield array

- 2- Estimating both propagating waves plus the positive decaying nearfield wave amplitudes of the nearfield array. Nine filters were designed using Eq.(3.17), in order to estimate the mentioned waves in the nearfield array. As shown in Figure 4.6 and Figure 4.7.

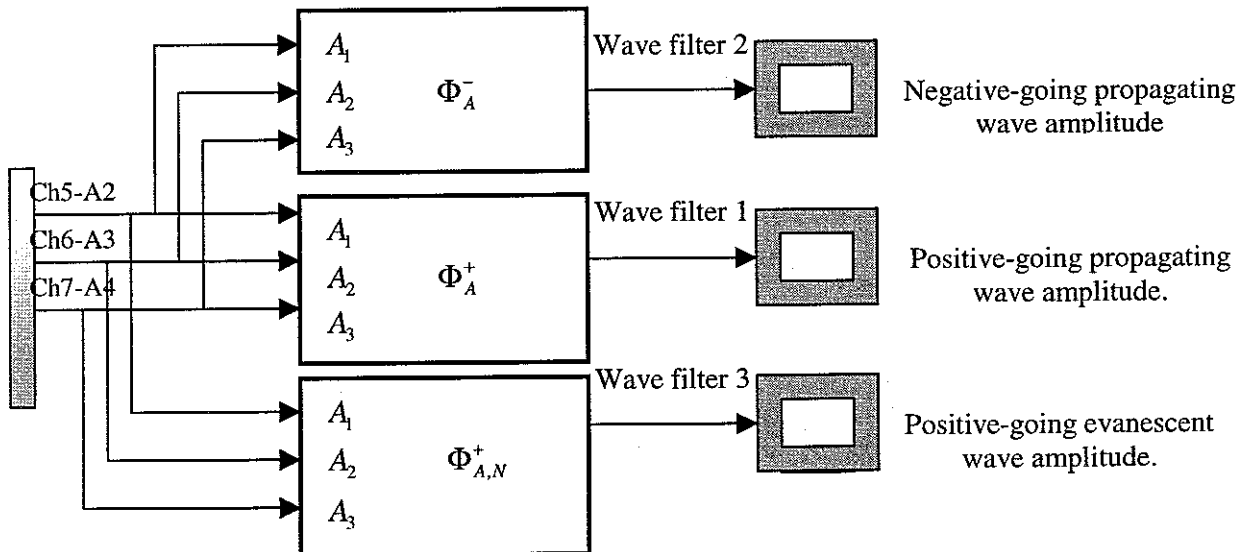


Figure 4.6. Simulink blocks of the Nearfield array

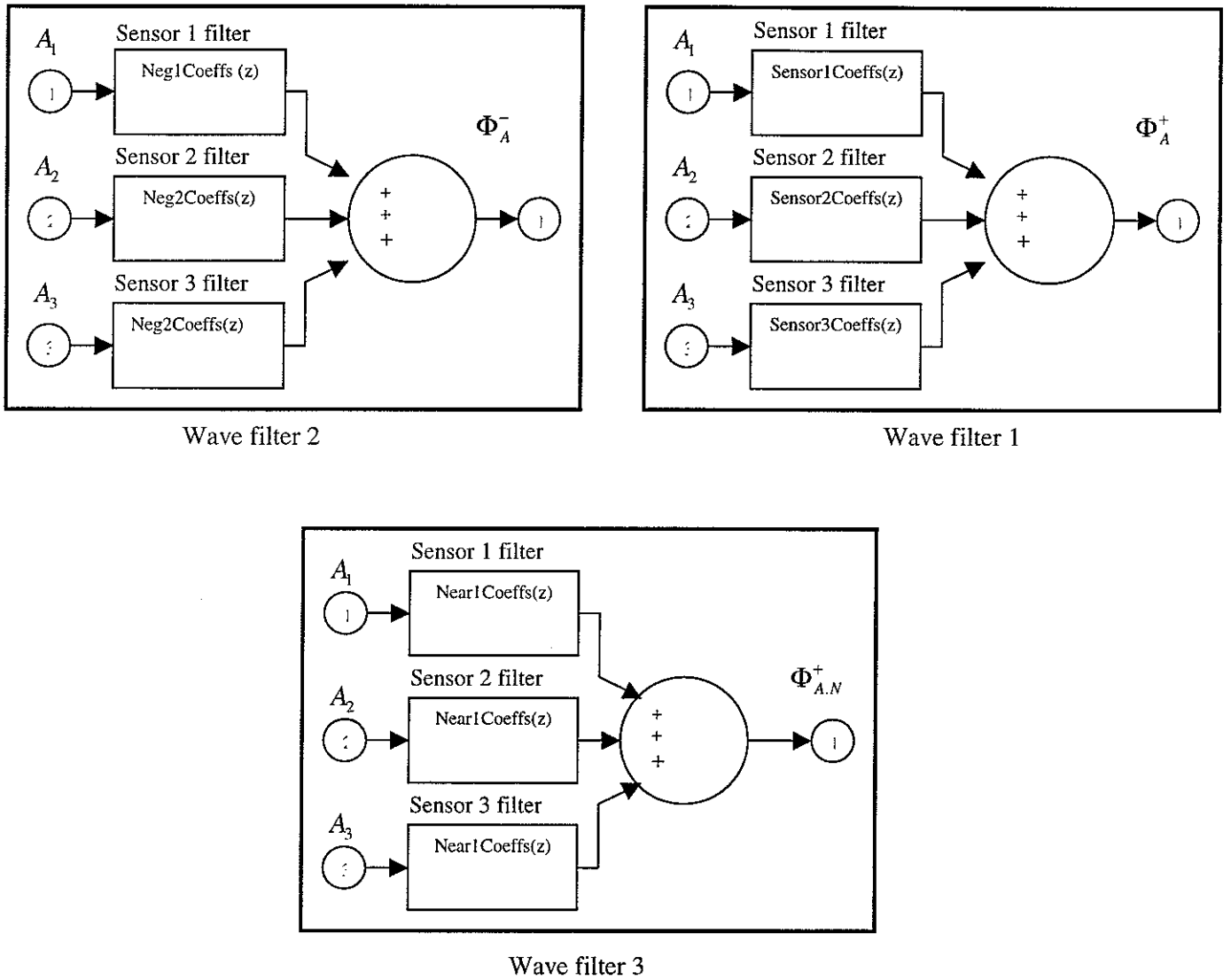


Figure 4.7. Simulink blocks for the FIR Filters used to estimate the wave amplitudes of the Nearfield array.

Matlab© is a powerful tool for digital signal processing and has many built in functions for designing digital filters. Three of these filter functions were used; these are *ellip*, *invfreqz* and *freqz*.

### 4.3 Reflection and Transmission Coefficients Due to Mass Discontinuity.

Consider a steel beam lying in the  $x$ -axis with a mass discontinuity at  $x=0$  (See Figure 4.8). The beam is suspended at 4 points along its length. Both ends were embedded in a sand box to reduce the reflection of waves. The beam was excited by a Ling V201 shaker in the farfield of the mass discontinuity that comprises two blocks of steel, each has the dimensions of  $98.5 \times 12.65 \times 25.4 \text{ mm}$  and accelerations measured using PCB type 352C22 accelerometers. Signals were generated and measurements processed in the frequency domain using an FFT analyser. Other equipment included a power amplifier and reconstruction filters.

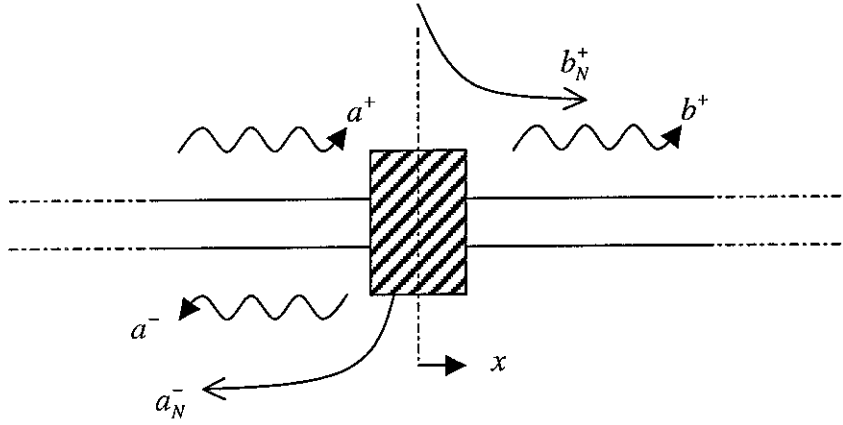


Figure 4.8. Infinite beam with mass discontinuity.

This section is set out in two subsections. The first one includes the numerical wave modelling of the reflection and transmission coefficients at a mass discontinuity attached to a beam, while the second section presents the experimental results in the frequency domain. Therefore, the validity of the theoretical derivations was investigated.

#### 4.3.1 Theoretical Wave Reflection and Transmission.

A positive – going wave  $a^+$  is incident upon a mass discontinuity and gives rise to transmitted  $b^+$  and reflected  $a^-$  waves, where

$$b^+ = ta^+, \quad a^- = ra^+, \quad a_N^- = r_N a^+, \quad b_N^+ = t_N a^+. \quad (4.4)$$

$t$  and  $r$  being the transmission and reflection coefficients, while the subscript N refers to nearfield waves.



The displacements of the beam  $w_-$  and  $w_+$  are given in Eq.(2.18). Reflection and transmission coefficients can be found by considering the continuity and equilibrium equations of the system. These are given by [5,13]

$$\begin{aligned} r &= \frac{-i\alpha}{4 + \alpha(1+i)} \\ t &= \frac{4 + \alpha}{4 + \alpha(1+i)} \\ r_n &= \frac{-\alpha}{4 + \alpha(1+i)} = t_N \end{aligned} \quad (4.5)$$

The dimensionless factor  $\alpha = 2\pi m / \rho A \lambda$ , relates the mass of the neutraliser  $m$  compared to the mass in one flexural wavelength of the beam.

The reflection coefficient of the propagating wave is the same as the reflection (and transmission) coefficient of the nearfield wave apart from a factor of  $-i$  times  $r$ , which is equivalent to  $270^\circ$  phase shift.

Figure 4.9 shows that the maximum reduction of an incident flexural wave using a mass discontinuity is only 3 dB as explained by [14].

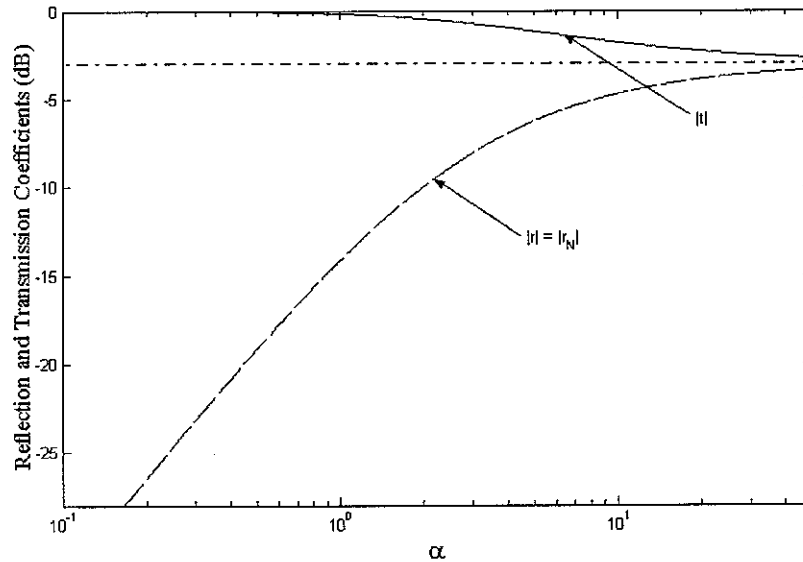


Figure 4.9. Transmission and reflection coefficients of flexural waves on an infinite Euler-Bernoulli beam with a mass discontinuity.

—————  $|t|$ ; .....  $|r|$ ; - - - - -  $|r_N|$ .

### 4.3.2 Estimating $r$ and $t$ in the frequency domain.

The reflection and transmission coefficients were found by estimating the propagating wave amplitudes in the frequency domain using an FFT analyser and four PCB type 352C22 accelerometers. The beam is excited in the frequency range from 0 – 1600Hz.

This section describes the method used in estimating  $r$  and  $t$ . Furthermore, a comparison between the theoretical modelling and the experimental investigation is presented.

From the basic knowledge of the wave decomposition approach (this is described in chapter two) together with the signal outputs of the four accelerometers, the reflection and transmission coefficients of the propagating waves\* can be estimated.

Two sensor arrays were used, where each contain two accelerometers with a separation of  $2\Delta$  as shown in Figure 4.10.

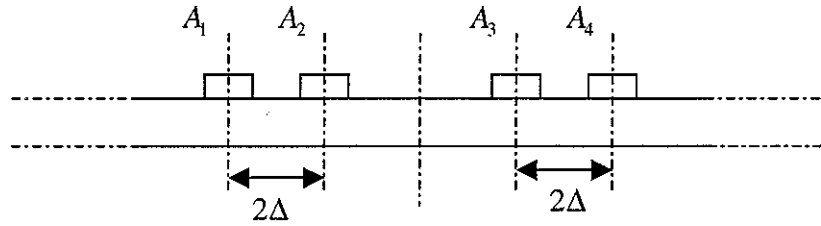


Figure 4.10. Beam structure comprising four accelerometers in two arrays.

The amplitudes of the positive- and negative-going propagating waves can be found from the first array. The accelerations  $A_1$  and  $A_2$  can be described as functions of  $a^+$  and  $a^-$ .

$$\begin{Bmatrix} A_1 \\ A_2 \end{Bmatrix} = \begin{bmatrix} e^{ik\Delta} & e^{-ik\Delta} \\ e^{-ik\Delta} & e^{ik\Delta} \end{bmatrix} \begin{Bmatrix} a^+ \\ a^- \end{Bmatrix}. \quad (4.6)$$

By solving the above equations for  $a^+$  and  $a^-$ , then the amplitude of the positive and negative propagating waves can be found below

$$\begin{Bmatrix} a^+ \\ a^- \end{Bmatrix} = \frac{1}{2i \sin(2k\Delta)} \begin{bmatrix} e^{ik\Delta} & -e^{-ik\Delta} \\ -e^{-ik\Delta} & e^{ik\Delta} \end{bmatrix} \begin{Bmatrix} A_1 \\ A_2 \end{Bmatrix}. \quad (4.7)$$

The same can be done for finding  $b^+$  and  $b^-$  in terms of  $A_3$  and  $A_4$ . Therefore, the transmission and reflection coefficients can be found by taking the four propagating waves into consideration.

---

\* These were estimated in the farfield-Nearfield waves are insignificant and have been ignored.

It is well known that

$$\begin{Bmatrix} b^+ \\ a^- \end{Bmatrix} = \begin{bmatrix} a^+ & b^- \\ b^- & a^+ \end{bmatrix} \begin{Bmatrix} t \\ r \end{Bmatrix}, \quad (4.8)$$

hence,

$$\begin{Bmatrix} t \\ r \end{Bmatrix} = \frac{1}{\Delta D} \begin{bmatrix} a^+ & -b^- \\ -b^- & a^+ \end{bmatrix} \begin{Bmatrix} b^+ \\ a^- \end{Bmatrix}, \quad (4.9)$$

where  $\Delta D = (a^+)^2 - (b^-)^2$  is the determinant.

The experimental set-up is shown in Figure 4.11. The distances between

- 1- the two accelerometers in each array,
  - 2- the source of disturbance and the centre line of the nearest sensor array, and
  - 3- the mass discontinuity and the centre line of each array
- were chosen carefully to minimise the effect of the nearfield waves at low frequencies.

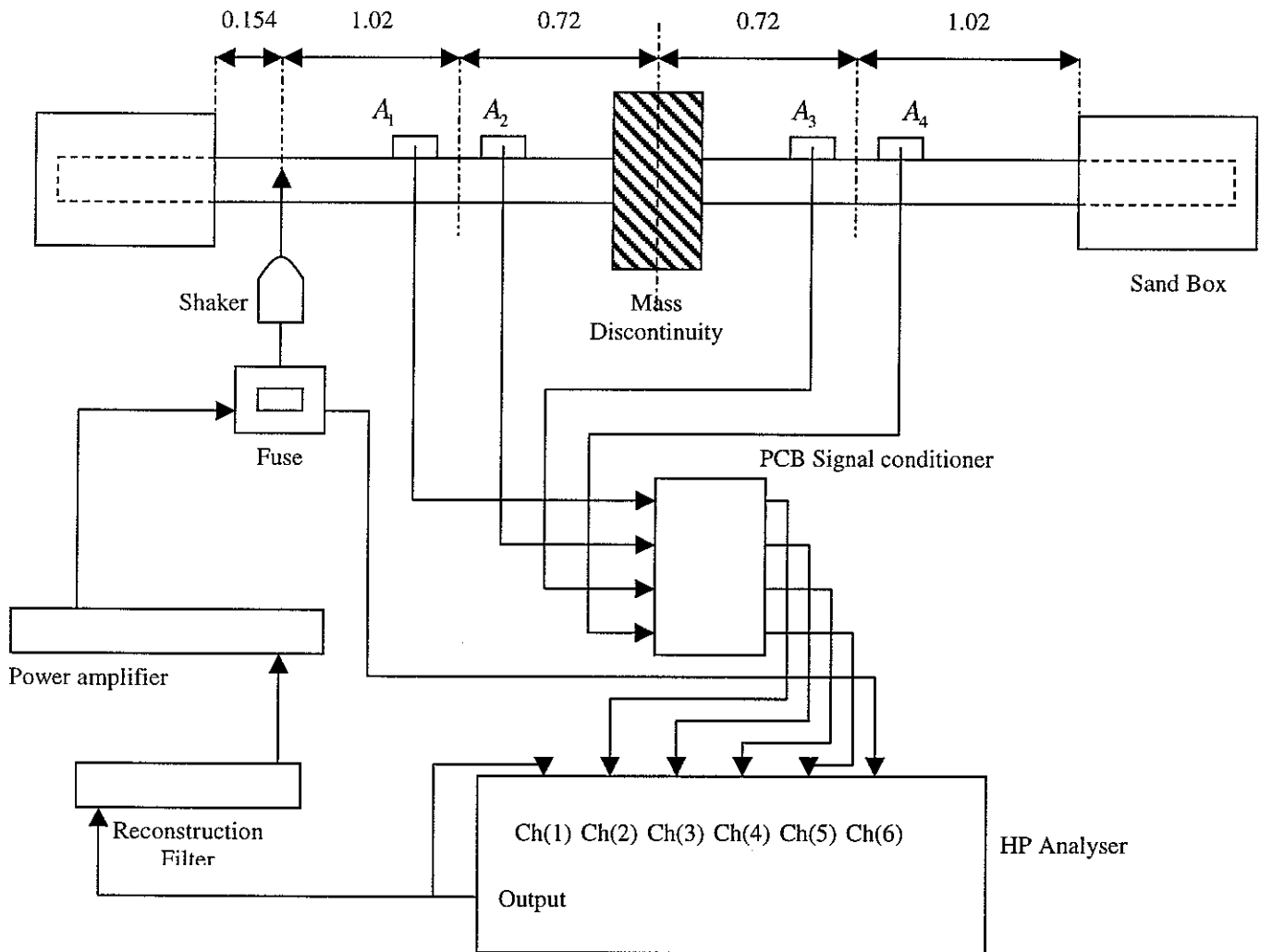


Figure 4.11. The experimental set-up used for estimating the propagating wave amplitudes. All dimensions in  $m$

In order to avoid nearfields at frequencies greater than 100Hz. The distance between shaker/sand box/mass and the sensor arrays was greater than the minimum wavelength  $\lambda_{\min} = 0.76m$  below which significant nearfields exist.

Also the distance between the sensors ( $2\Delta$ ) was chosen carefully for signal conditioning matter. Thus the ideal distance should not be more than  $0.0672m$  (the implemented  $2\Delta = 0.04$ ).

The mass ratio  $\alpha$  between the attached mass and the mass of one wavelength of the beam as a function of frequency was  $0.1604\sqrt{f}$ .

## 5. RESULTS AND DISCUSSION.

This chapter presents the results of the experiments described in the previous chapter in two sections. A comparison between the measured wave amplitudes due to discrete frequency excitation is discussed in the first section. The estimated wave amplitudes due to broadband excitation are also compared in this section. The second section investigates the validity of the theoretical modelling of the transmission coefficient due to mass discontinuity.

### 5.1 Real-Time Comparison of the Estimated Wave Amplitudes.

The wave amplitudes are measured by digitally filtering and combining the outputs of an array of accelerometers. The filters are designed in the frequency domain using a wave decomposition approach, and implemented in the time domain as FIR filters. This has been explained theoretically and experimentally in chapters three and four respectively.

#### 5.1.1 Discrete frequency excitation.

The effect of changing the time delay term  $(n_d)^*$  on estimating the wave amplitudes is investigated in this section. Then a comparison between the effectiveness of both approaches in estimating the wave amplitudes in the farfield is considered.

The length of the filter was found to have an insignificant effect on estimating the wave amplitudes as shown in Figure 5.1 for the first configuration (See Figure 4.3 (a)).

---

\* There are a number of ways of designing FIR filters. The 'time delay' approach adopted here was described in [1].

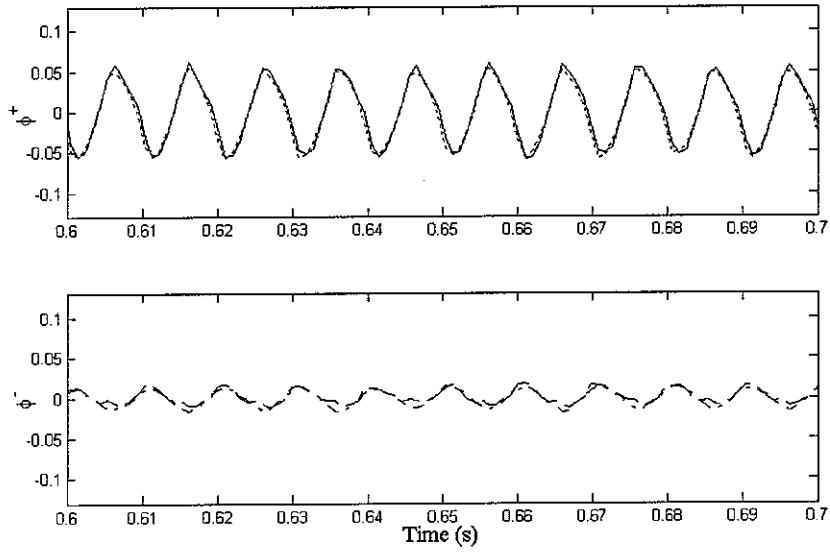


Figure 5.1. The effect of changing  $n_d$  on estimating the wave amplitudes of the first configuration.

—  $\phi^+$ ,  $n_d = 5$ ;      .....  $\phi^+$ ,  $n_d = 15$ ;  
 - - -  $\phi^-$ ,  $n_d = 5$ ;      - · -  $\phi^-$ ,  $n_d = 15$ .

Far- and nearfield approaches were found to estimate the same wave amplitudes in the farfield of the first configuration, although the nearfield approach takes the evanescent wave into account. Some results are shown in Figure 5.2.

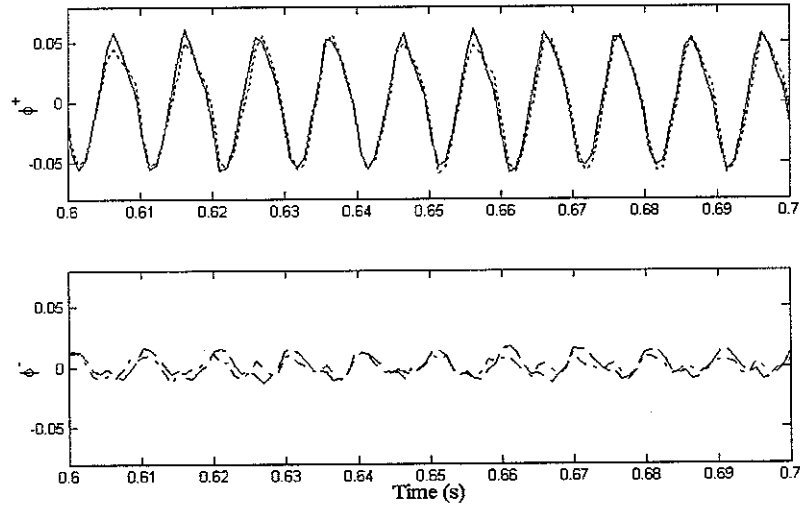


Figure 5.2. Comparison between the propagating waves estimated by both approaches for the first configuration.  $n_d = 5$ ,  $f = 100\text{Hz}$ .

—  $\phi^+$ , of farfield array; .....  $\phi^+$ , of nearfield array;  
 - - -  $\phi^-$ , of farfield array; - · -  $\phi^-$ , of nearfield array.

Very small amount of the incident propagating wave  $\phi^+$  is reflected back from the sandbox as explained previously for the first configuration (Figure 4.3 (a)). This is illustrated in Figure 5.3.

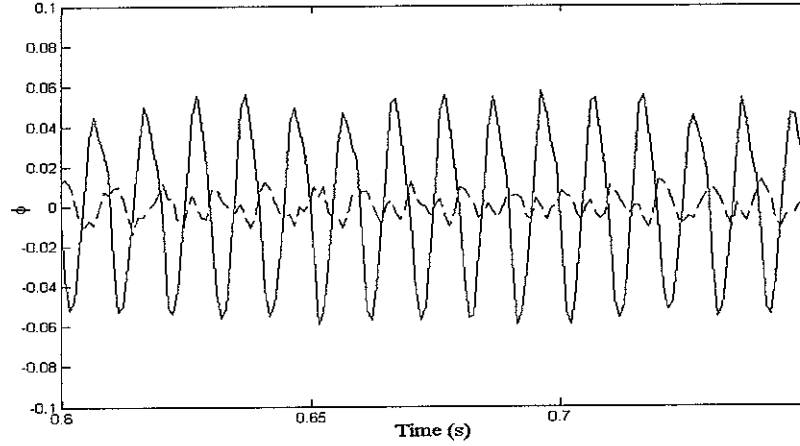


Figure 5.3. The propagating waves of the first configuration,  $n_d = 5$ ,  $f = 100\text{Hz}$ .

—————  $\phi^+$ ;      - - - - -  $\phi^-$ .

The amplitudes estimated at the two different  $n_d$  are very much the same. This has been verified for both farfield (2 – sensor) and nearfield (3 – sensor) arrays.

For the second configuration (Figure 4.3 (b)), Figure 5.4 (a) shows that the amplitude of the incident propagating waves estimated from both arrays nearly have the same amplitudes as expected. Furthermore, the amplitudes of the reflected propagating waves  $\phi^-$  are nearly 1/3 those of the incident waves as illustrated in Figure 5.4 (b). The estimates from both arrays have very close wave amplitudes for the negative propagating wave. It was found that the evanescent wave estimated from the nearfield array located at the free end has an amplitude comparable to that of the positive – going waves. This is shown in Figure 5.4 (c).

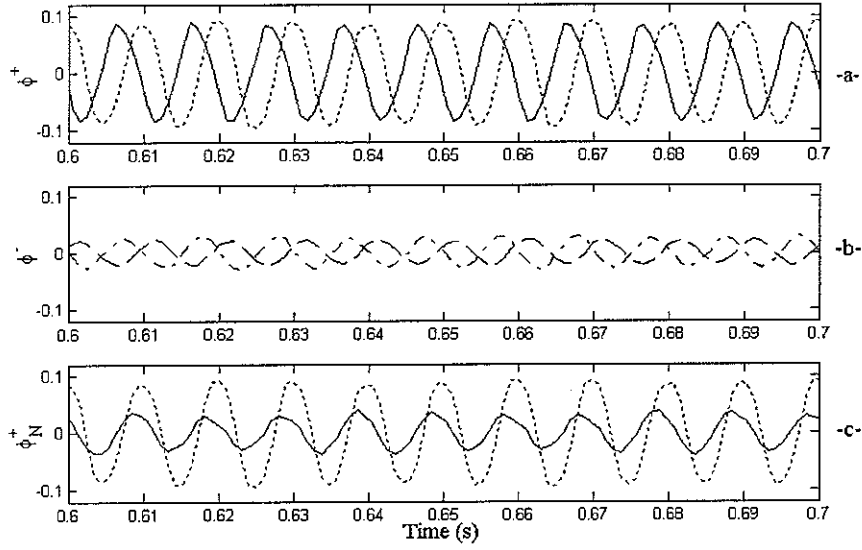


Figure 5.4. The flexural wave amplitudes estimated from both arrays of the second configuration,  $n_d = 5$ ,  $f = 100\text{Hz}$ .

- (a) Positive propagating waves: —  $\phi^+$ , of farfield array; .....  $\phi^+$ , of nearfield array;  
(b) Negative propagating waves: -----  $\phi^-$ , of farfield array; - - - - -  $\phi^-$ , of nearfield array.  
(c) Positive propagating and evanescent waves: —  $\phi_N^+$ ; .....  $\phi^+$  of nearfield array.

Although the wave amplitudes were found to be the same, there is a distinct phase different between the estimated waves from both approaches. Where various filters have been used in estimating the different flexural waves.

### 5.1.2 Broadband excitation.

The spectral power density is used for the comparison between wave amplitudes in the third configuration.

Broadband excitation in the 51–461Hz frequency band is supplied. The sensors were mounted as shown in Figure 4.3 (c).

The 3 – sensor array is mounted in the nearfield at the end of the beam, while the 2 – sensor array is once again in the farfield.

This arrangement enables the broadband performance to be assessed. In figure 5.5 (a), the spectral densities of the estimated propagating wave amplitudes are compared. The spectral densities of both positive and negative going propagating wave amplitudes estimated using both near – and farfield arrays, are nearly equal, as one would expect since there is little energy dissipation in this region of the beam.





## 5.2 Investigating the Validity of the Theoretical Modelling of the Transmission Coefficient $t$ Due to Mass Discontinuity.

A comparison between the theoretical and experimental estimation of the transmission of the incident propagating waves due to mass discontinuity is discussed in this section. Both the theoretical and experimental methods for estimating the reflection and transmission of the flexural waves were explained in details in section 4.3.

Figure 5.6 shows that at high frequencies the theory becomes irrelevant to the experimental results. However, the wavelength of the nearfield waves gets larger and becomes more significant by increasing the excitation frequency.

A comparable match may exist between the theoretical and experimental estimation of the transmission coefficient  $|t|$  over a frequency range of 100 – 400 Hz.

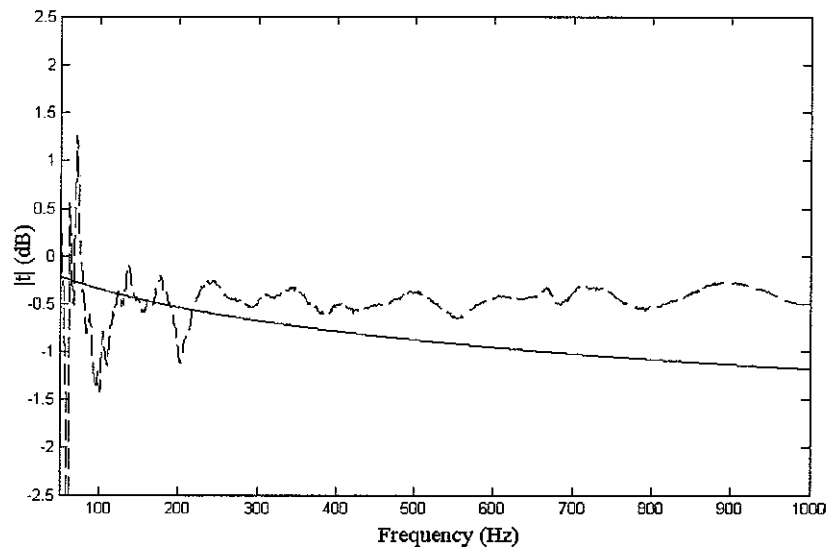


Figure 5.6. Comparison between the theoretical and experimental attenuation occurred to the incident wave due to mass discontinuity.

—————  $|t|$  (Theoretical); - - - - -  $|t|$  (Experimental).

The accuracy of the experimental result was verified. This is illustrated in Figure 5.7 below.

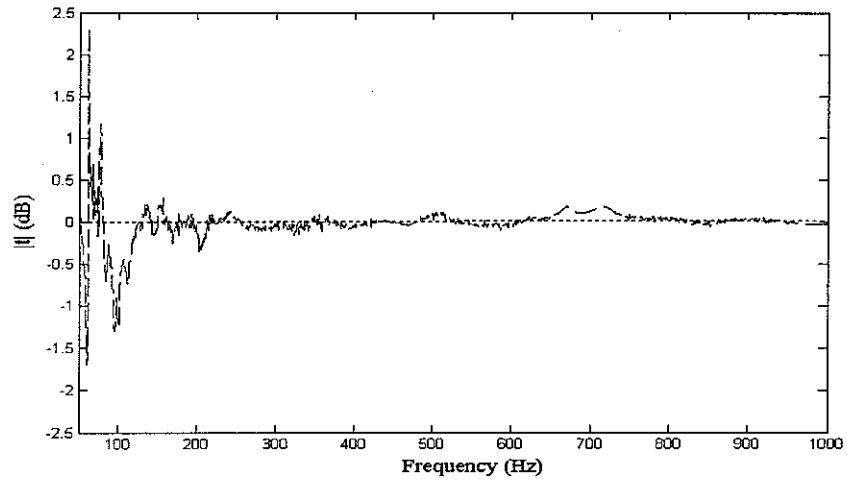


Figure 5.7. Comparison between the theoretical and experimental attenuation occurred to the incident wave. No mass is attached experimentally.  
.....  $|r|$  (Theoretical estimation-mass is attached);-----  $|t|$  (Experimental estimation).

Figure 5.7 compares the experimental estimation for no mass attached with the theoretical one, which is assumed to be a straight line (reflection is assumed to be insignificant).

Conservation of energy has been satisfied in the experimental results, where it was found that  $|r|^2 + |t|^2 \cong 1$ . The existence of the attached mass has slightly affected the energy verification as a result of incorporating more evanescent waves. This is shown in Figure 5.8 below.

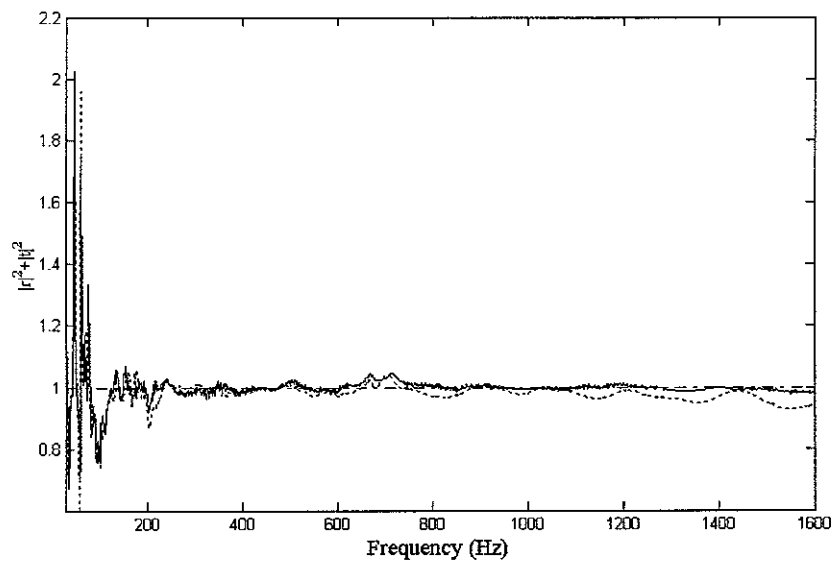


Figure 5.8. Satisfying the conservation of energy  $|r|^2 + |t|^2 = 1$ .  
(a) Experimentally: ——— no mass attached; ..... mass is attached.  
(b) Theoretically: - - - - -

## **6- CONCLUSION AND DISCUSSION.**

This chapter highlights some general remarks of the previous chapters and the potential future work upon the results obtained from this memorandum.

### **6.1 General Concluding Remarks.**

The amplitudes of the flexural waves were estimated in real-time including nearfields. This will allow measurements to be taken close to the force, boundary, or discontinuity from which the nearfield arises.

The ratio of both reflected and transmitted waves to the incident waves were estimated in the frequency domain. Reasonable match obtained with the theoretical modelling over a certain frequency range.

Instantaneous values of intensity amplitude can be obtained easily as function of time.

### **6.2 Future Work.**

The estimated wave amplitudes will be used as a cost function in a potential control system for an adaptive – passive neutraliser.

The match between the theoretical and experimental reflection and transmission coefficients gives some confidence in the numerical modelling for more complicated discontinuities.

## APPENDICES

### A1.0 The boundary conditions of the four common cases of beam ends.


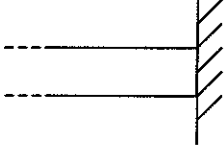
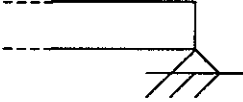
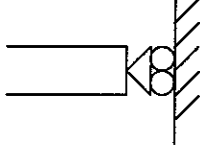
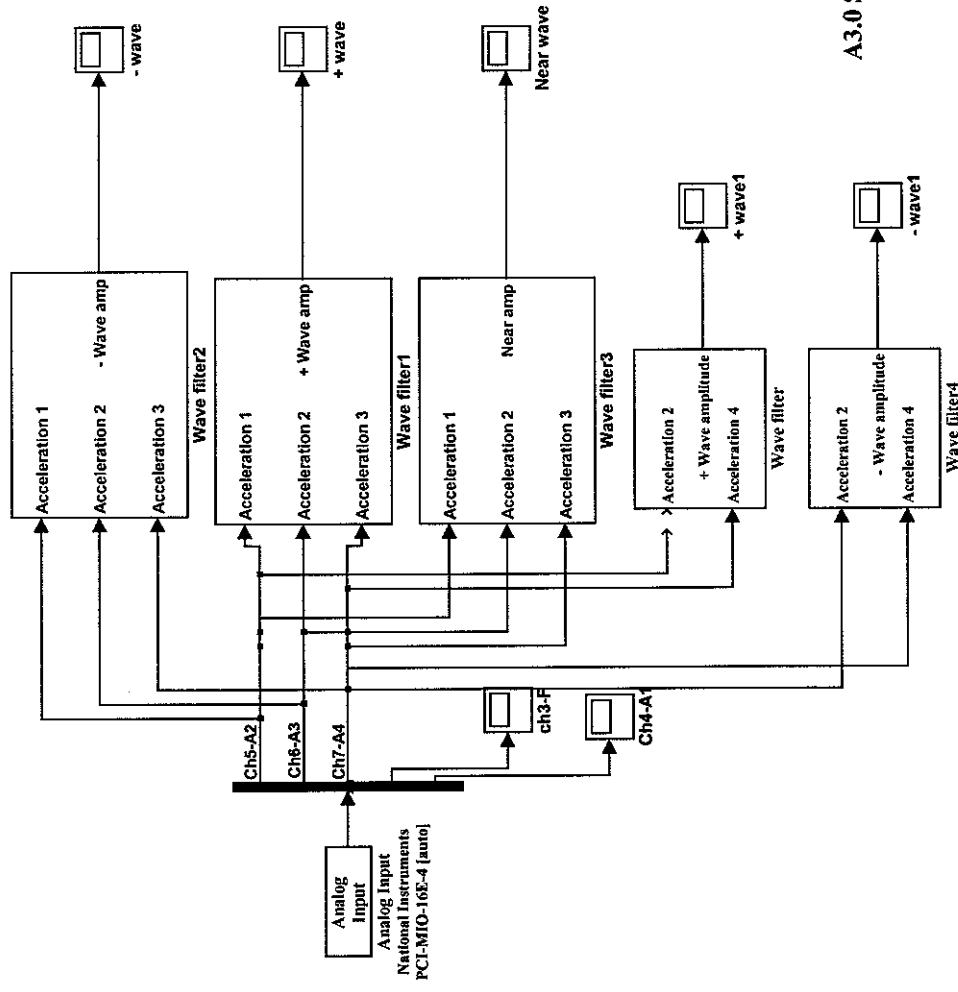
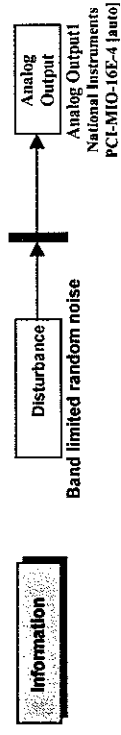
End Status	Diagram at $x = 0$	First Condition	Second Condition
Free End		$\frac{\partial^2 w}{\partial x^2} = 0$	$\frac{\partial^3 w}{\partial x^3} = 0$
Clamped End		$w = 0$	$\frac{\partial w}{\partial x} = 0$
Simple Supported		$w = 0$	$\frac{\partial^2 w}{\partial x^2} = 0$
Sliding		$\frac{\partial w}{\partial x} = 0$	$\frac{\partial^3 w}{\partial x^3} = 0$

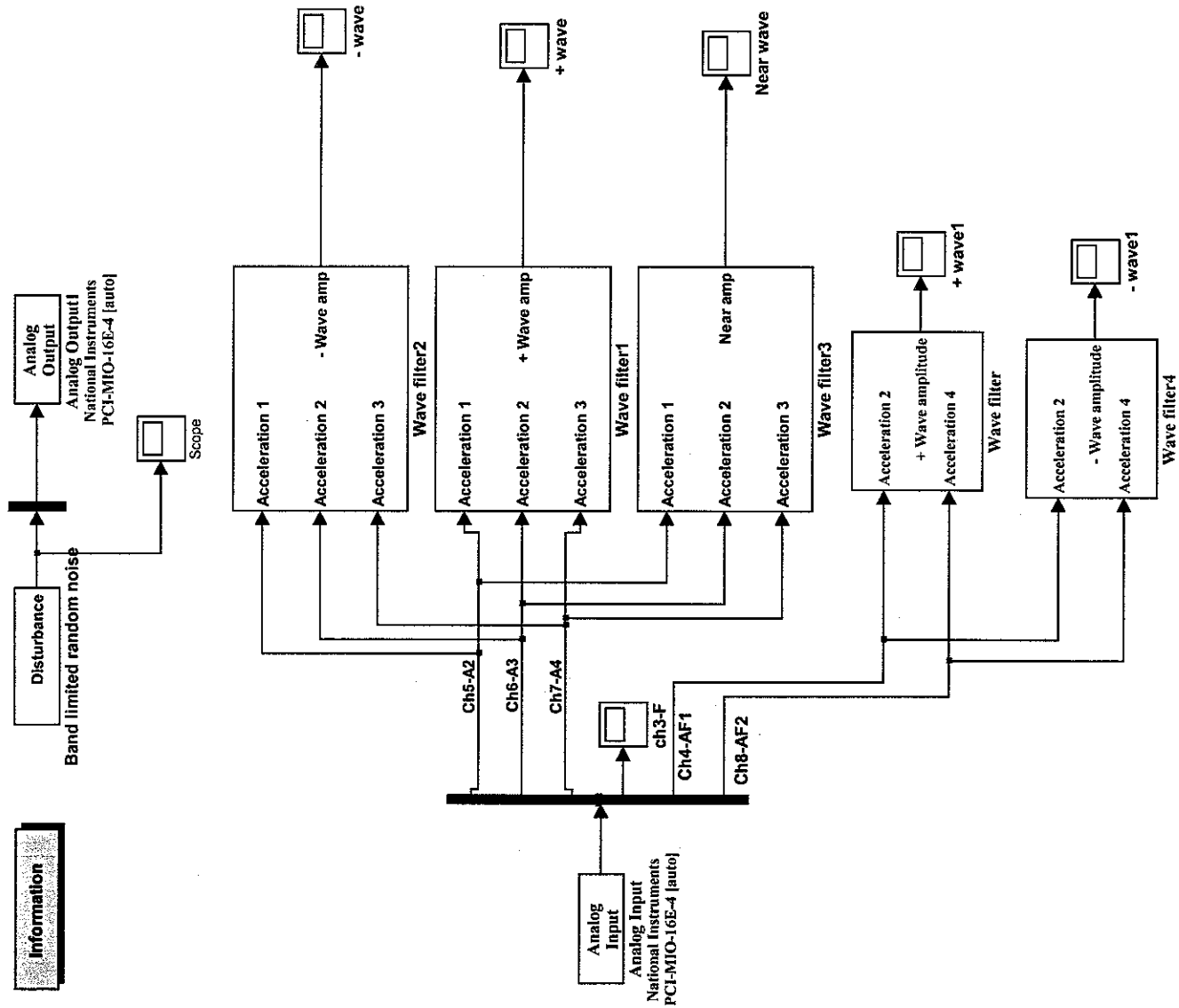
Table A1.0

## A2.0 Experimental equipment.

Equipment	Specifications
<u>Disturbance and control signal generation</u>	1GHz Intel Pentium III processor with 256k cash.
<b>Data Acquisition Board</b>	National Instruments PCI-MIO-16E-4 A-D: 16 single ended or 8 different inputs. D-A: 2 Outputs. Input ranges: 0-10V, +/-10V Gains: Various. Output ranges: 0-10V, +/-10V
<b>Reconstruction filter: D-A</b>	Type VBF8, 0.01Hz – 100kHz Dual variable filter, s/n 56198
<b>Disturbance Shaker</b>	Ling Dynamic Systems (LDS) – V201 SN/69439/5.
<b>Amplifier</b>	Ariston, Ax-910 integrated Amplifier /SN/735-Ax910-0700-0142
<b>Sensors used</b>	<p><b>PCB (352C22) Types</b></p> <ul style="list-style-type: none"> <li>- A1      s/n 35914</li> <li>- A2      s/n 35911</li> <li>- A3      s/n 35909</li> <li>- A4      s/n 35910</li> <li>- A5      s/n 36100</li> </ul>
<b>Signal conditioner</b>	Two PSC Sensor Signal conditioners, Model/441A2, GRP/64106/SN/748 and SN/749.



**A3.0 Simulink Block Diagram for the estimated wave amplitude of the three configuration**  
**a- For the First Configuration**



**b- For the second and third Configurations**



## A4.0 The Matlab M-files of the designed wave filters.

### 1- wave.m

```
% *****
% ((FARFIELD CASE))-(TWO SENSORES))
% wave.m initialises stuff for the Simulink model using acceleration inputs
% to estimate Acceleration wave amplitudes
%
% Assumes 2 acceleration sensors, separation delta
% Frequencies at multiples of 1 Hz
% *****
%Modified by HEK on 04-02-02

% *****
% Data
% *****
SampleFreq = input('Enter Sample Frequency: '); % sampling frequency, power of 2
SineFreq = input('Enter the sine Frequency Required (Hz): ');
Alpha=0.8269; % constant relating k to sqrt(f)
LossFactor = input('Enter Loss Factor: '); % loss factor (imag proportion of wavenumber
% *****
% Frequency and wavenumber vectors
% *****
freq=[0:SampleFreq-1]'; % frequency, Hz
w=freq(1:SampleFreq/2)*2*pi/SampleFreq; % freq rad/sec: pi = Nyquist freq
k=Alpha*(1-i*LossFactor)*sqrt(freq(1:SampleFreq/2)); % wavenumber

% *****
% Design bandpass filter for disturbance
% *****
[Bandb,Banda]=ellip(5,0.5,50,[0.2 0.8]);

% *****
% Wave amplitude filter stuff
% *****
NDelay=5; % number of delay terms: filter length = 2*NDelay + 1
Delta=0.1200; % sensor spacing (m)
coeff % find wave amplitude FIR filter coefficients

% *****
% Control filter
% *****
ControlFIR=[1];
```

## 2- coeff.m

```
% *****
% ((FARFIELD CASE))-((TWO SENSORES))
% coeff.M finds FIR filters for ACCELERATION WAVE error sensors.
%
% Called from wave.m, in which the required data is defined.
% Assumes 2 acceleration sensors; neglects damping, uses
% "time delay" method
% Weights 'loose' ends of frequency range to zero
% *****
% Modifid by Hassan El-Khatib - 3th-02-02

nb=2*NDelay;          % order of numerator (FIR/IIR): there are nb+1 coeffs
na=0;                 % order of denominator (IIR only): there are na+1 coeffs
                        % na = 0 gives FIR filter
EI = 232.05;          % Rigidity of the beam

% *****
% Frequency weights: set weights at ends of frequency range to zero
% *****
zeroproportion=0.1;   % proportion of freq range to "cut-off" which is
zero weighted
nzeros=round(zeroproportion*length(w)); % number of points for zero weighting
wt=[zeros(1,nzeros),ones(1,max(size(w))-(2*nzeros)),zeros(1,nzeros)];
% *****
% Define ideal frequency responses
% *****
kd2=k*Delta/2;        % k * delta /2, neglecting damping

H1=1./(4*cos(kd2)); % ideal frequency responses, modified from velocity to acceleration response
H2=i./(4*sin(kd2)); % ideal frequency responses, modified from velocity to acceleration response

H1(1)=H1(2);          % eliminate 'infinities'
H2(1)=H2(2);

% *****
% Modify ideal frequency responses with 'bandpass' characteristic
% *****
endshape=hanning(200,'periodic');
shape=[endshape(1:100),ones(1,max(size(w))-200),endshape(101:200)]';
```

Continue coeff.m

```

% *****
%
% FIR implementation (time delay)
% *****
[WaveSumCoeffs,a]=invfreqz(H1.*exp(-i*w*NDelay),w,nb,na,wt); % FIR filter, time delayed
% ndelay steps

[WaveDiffCoeffs,a]=invfreqz(H2.*exp(-i*w*NDelay),w,nb,na,wt); % FIR filter, time delayed
% ndelay steps

[H1imp,wimp]=freqz(WaveSumCoeffs,a,length(w)); % implemented freq response Ht1

[H2imp,wimp]=freqz(WaveDiffCoeffs,a,length(w)); % implemented freq response Ht2

H1imp=H1imp.*exp(i*w*NDelay); % time delayed: phase removed (for comparison)
H2imp=H2imp.*exp(i*w*NDelay); % time delayed: phase removed (for comparison)

figure
semilogy(w,abs(H1),'--',wimp,abs(H1imp))
figure
semilogy(w,abs(H2),wimp,abs(H2imp))

```

### 3 – Near.m

```

% *****
%
% ((NEAR FIELD CASE))-(THREE SENSORES))
% Near.m initialises stuff for the experimental AVC model INCLUDING NEARFIELDS
%
% Assumes 3 Acceleration sensors, separation delta
% Currently written so that frequencies at multiples of 1 Hz
% Wave amplitude estimated at CENTRE of the 3-sensor array
%
% Allows you to specify WaveFilterType to change way of estimating wave amp
%
% HEK 11/01/02 - Modified in 04/02/02
% *****

% *****
% Data
% *****
SampleFreq = input('Enter Sample Frequency: '); % sampling frequency, power of 2
SampleTime=1/SampleFreq; % sample time
Alpha=0.8269; % constant relating k to sqrt(f)
LossFactor = input('Enter Loss Factor: '); % loss factor (imag proportion of wavenumber)-
% represent damping

% *****
% Frequency and wavenumber vectors
% *****
freq=[0:SampleFreq-1]'; % frequency, Hz
k=Alpha*(1-i*LossFactor)*sqrt(freq(1:SampleFreq/2)); % relationship between wavenumber and
% frequency
w=freq(1:SampleFreq/2)*2*pi/SampleFreq; % freq rad/sec: pi = Nyquist freq

```

Continue Near.m

```

% *****
% Design bandpass filter for disturbance
% *****
Banda=1; % set to one for no bandpassing of source
Bandb=1;
[Bandb,Banda]=ellip(5,0.5,50,[0.2 0.8]); % prescribe limits if you want the disturbance band-limited

% *****
% Wave amplitude filter stuff
% *****
NDelay=5; % number of delay terms: filter length = 2*NDelay + 1
Delta=0.060; % sensor spacing (wavelengths at Nyquist frequency)
WaveFilterType=0; % type of wave filter:
% 0 G on its own
% 1 i*w*G
% 2 i*w*G*sqrt(-i)
NearCoeffs % find wave amplitude FIR filter coefficients

% *****
ControlFIR=[1];

```

#### 4- NearCoeffs.m

```

% *****
% ((NEAR FIELD CASE))-((THREE SENSORES))
% NearCoeffs.m finds FIR filters for 3 ACCELERATION WAVE errors
% Sensors with a nearfield
% Called from Near.m, in which the required data is defined.
% Assumes 3 acceleration sensors; neglects damping, uses "time delay" method
% Weights 'loose' ends of frequency range to zero
% Wave amplitude is estimated at sensor array centre
%
% WaveFilterType is set to determine actually what filter is implemented
%
% HEK 11/01/02, modified in 15/01/02
% *****

nb=2*NDelay; % order of numerator (FIR/IIR): there are nb+1 coeffs
na=0; % order of denominator (IIR only): there are na+1 coeffs
% na = 0 gives FIR filter
EI = 232.05; % Rigidity of the beam

% *****
% Frequency weights: set weights at ends of frequency range to zero
% *****
wt=1+w*0; % weights, all set = 1
zeroproportion=0.1; % proportion of freq range to "cut-off" which is zero weighted
nzeros=round(zeroproportion*length(w)); % number of points for zero weighting
wt=[zeros(1,nzeros),ones(1,max(size(w))-(2*nzeros)),zeros(1,nzeros)];

```

Continue NearCoeffs.m

```

% *****
%
% Define ideal frequency responses
% *****
HQ1=i.*EI*k.^3./(w.^2); % Ideal Frequency response of the shear force.Modified to acc
HQ2=-EI*k.^3./(w.^2); % Modified on the date above.
HM=EI*k.^2./(w.^2); % Ideal Frequency response of bending moment.Modified to acc
HV = -i./w; % Ideal Frequency response of velocity.Modified to acc
HS1 = k./w; % Ideal Frequency response of angular velocity.Modified to acc
HS2 = i.*k./w; % Modified on the date above.

HQ1(1)=HQ1(2);
HQ2(1)=HQ2(2);
HV(1)=HV(2);
HM(1)=HM(2);
HS1(1)=HS1(2);
HS2(1)=HS2(2);
% *****
%
% Modify ideal frequency responses with 'bandpass' characteristic
% *****
endshape=hanning(200,'periodic');
shape=[endshape(1:100),ones(1,max(size(w))-200),endshape(101:200)'];

ka=k*Delta; % k * spacing delta
G11=[];G12=[];G13=[];
G21=[];G22=[];G23=[];
G31=[];G32=[];G33=[];

for jfreq=1:length(w),
    s=[exp(i*ka(jfreq)) exp(-i*ka(jfreq)) exp(ka(jfreq));
        1 1 1;
        exp(-i*ka(jfreq)) exp(i*ka(jfreq)) exp(-ka(jfreq))];
        % sensor matrix at given frequency
        % invert.....
    invs=inv(s);
    G11=[G11;invs(1,1)]; % ... and extract the propagating wave elements & near field in G
    G12=[G12;invs(1,2)];
    G13=[G13;invs(1,3)];
    G21=[G21;invs(2,1)];
    G22=[G22;invs(2,2)];
    G23=[G23;invs(2,3)];
    G31=[G31;invs(3,1)];
    G32=[G32;invs(3,2)];
    G33=[G33;invs(3,3)];

end

G11(1)=G11(2); % get rid of NaN's
G12(1)=G12(2);
G13(1)=G13(2);
G21(1)=G21(2);
G22(1)=G22(2);
G23(1)=G23(2);
G31(1)=G31(2);
G32(1)=G32(2);
G33(1)=G33(2);

```

```

% *****
%
% Find frequency responses for chosen filter type
% *****
if WaveFilterType==0      %      0      G on its own
    G11=G11;
    G12=G12;
    G13=G13;

elseif WaveFilterType==1      %      1      i*w*G
    G11=i*w.*G11;
    G12=i*w.*G12;
    G13=i*w.*G13;

elseif WaveFilterType==2      %      2      i*w*G*sqrt(-i)
    G11=i*w.*G11*sqrt(-i);
    G12=i*w.*G12*sqrt(-i);
    G13=i*w.*G13*sqrt(-i);

end

% *****
%
% FIR implementation (time delay)
% *****

% The positive going wave filter design.
[Sensor1Coeffs,a]=invfreqz(G11.*exp(-i*w*NDelay),w,nb,na,wt); % FIR filter, time delayed ndelay
% steps
[Sensor2Coeffs,a]=invfreqz(G12.*exp(-i*w*NDelay),w,nb,na,wt); % FIR filter, time delayed ndelay
% steps
[Sensor3Coeffs,a]=invfreqz(G13.*exp(-i*w*NDelay),w,nb,na,wt); % FIR filter, time delayed ndelay
% steps

% The negative going wave filter design.
[Neg1Coeffs,a]=invfreqz(G21.*exp(-i*w*NDelay),w,nb,na,wt); % FIR filter, time delayed ndelay
% steps
[Neg2Coeffs,a]=invfreqz(G22.*exp(-i*w*NDelay),w,nb,na,wt); % FIR filter, time delayed ndelay
% steps
[Neg3Coeffs,a]=invfreqz(G23.*exp(-i*w*NDelay),w,nb,na,wt); % FIR filter, time delayed ndelay
% steps

% The near field wave filter design.
[Near1Coeffs,a]=invfreqz(G31.*exp(-i*w*NDelay),w,nb,na,wt); % FIR filter, time delayed ndelay
% steps
[Near2Coeffs,a]=invfreqz(G32.*exp(-i*w*NDelay),w,nb,na,wt); % FIR filter, time delayed ndelay
% steps
[Near3Coeffs,a]=invfreqz(G33.*exp(-i*w*NDelay),w,nb,na,wt); % FIR filter, time delayed ndelay
% steps

[ShearCoeffs1,a]=invfreqz(HQ1.*exp(-i*w*NDelay),w,nb,na,wt); % FIR filter, time delayed ndelay
% steps
[ShearCoeffs2,a]=invfreqz(HQ2.*exp(-i*w*NDelay),w,nb,na,wt); % FIR filter, time delayed ndelay
% steps
[MomentCoeffs,a]=invfreqz(HM.*exp(-i*w*NDelay),w,nb,na,wt); % FIR filter, time delayed ndelay
% steps
[VelocityCoeffs,a]=invfreqz(HV.*exp(-i*w*NDelay),w,nb,na,wt); % FIR filter, time delayed ndelay
% steps
[AngularCoeffs1,a]=invfreqz(HS1.*exp(-i*w*NDelay),w,nb,na,wt); % FIR filter, time delayed ndelay
% steps
[AngularCoeffs2,a]=invfreqz(HS2.*exp(-i*w*NDelay),w,nb,na,wt); % FIR filter, time delayed ndelay

```

```

% steps
[G11imp,wimp]=freqz(Sensor1Coeffs,a,length(w)); % implemented freq response G11
[G12imp,wimp]=freqz(Sensor2Coeffs,a,length(w)); % implemented freq response G12
[G13imp,wimp]=freqz(Sensor3Coeffs,a,length(w)); % implemented freq response G13

[G21imp,wimp]=freqz(Neg1Coeffs,a,length(w)); % implemented freq response G21
[G22imp,wimp]=freqz(Neg2Coeffs,a,length(w)); % implemented freq response G22
[G23imp,wimp]=freqz(Neg3Coeffs,a,length(w)); % implemented freq response G23

[G31imp,wimp]=freqz(Near1Coeffs,a,length(w)); % implemented freq response G31
[G32imp,wimp]=freqz(Near2Coeffs,a,length(w)); % implemented freq response G32
[G33imp,wimp]=freqz(Near3Coeffs,a,length(w)); % implemented freq response G33

[HQ1imp,wimp]=freqz(ShearCoeffs1,a,length(w)); % implemented freq response HtQ
[HQ2imp,wimp]=freqz(ShearCoeffs2,a,length(w)); % implemented freq response HtQ
[HMimp,wimp]=freqz(MomentCoeffs,a,length(w)); % implemented freq response HtM
[HVimp,wimp]=freqz(VelocityCoeffs,a,length(w)); % implemented freq response HtV
[HS1imp,wimp]=freqz(AngularCoeffs1,a,length(w)); % implemented freq response HtS
[HS2imp,wimp]=freqz(AngularCoeffs2,a,length(w)); % implemented freq response HtS

G11imp=G11imp.*exp(i*w*NDelay); % time delayed: phase removed (for comparison)
G12imp=G12imp.*exp(i*w*NDelay); % time delayed: phase removed (for comparison)
G13imp=G13imp.*exp(i*w*NDelay); % time delayed: phase removed (for comparison)

G21imp=G21imp.*exp(i*w*NDelay); % time delayed: phase removed (for comparison)
G22imp=G22imp.*exp(i*w*NDelay); % time delayed: phase removed (for comparison)
G23imp=G23imp.*exp(i*w*NDelay); % time delayed: phase removed (for comparison)

G31imp=G31imp.*exp(i*w*NDelay); % time delayed: phase removed (for comparison)
G32imp=G32imp.*exp(i*w*NDelay); % time delayed: phase removed (for comparison)
G33imp=G33imp.*exp(i*w*NDelay); % time delayed: phase removed (for comparison)

HQ1imp=HQ1imp.*exp(i*w*NDelay); % time delayed: phase removed (for comparison)
HQ2imp=HQ2imp.*exp(i*w*NDelay); % time delayed: phase removed (for comparison)
HMimp=HMimp.*exp(i*w*NDelay); % time delayed: phase removed (for comparison)
HVimp=HVimp.*exp(i*w*NDelay); % time delayed: phase removed (for comparison)
HS1imp=HS1imp.*exp(i*w*NDelay); % time delayed: phase removed (for comparison)
HS2imp=HS2imp.*exp(i*w*NDelay); % time delayed: phase removed (for comparison)

% clear na nb wt zeroproportion nzeros a kd2

```

End of NearCoeffs.m

## REFERENCES

- 1- B. R. MACE and C. R. HALKYARD 1998 *IRL Report No. 91406-98-1*. Structural Acoustic Variables as Cost Functions in Active Vibration Control.
- 2- B. R. MACE and C. R. HALKYARD 1999 *IRL Report No. 91406-99-1*. Active Wave Control: Modelling & Simulation.
- 3- C. R. HALKYARD and B. R. MACE 1999 *IRL Report No. 91406-99-2*. Active Wave Control: Experimental Results.
- 4- B. R. MACE and C. R. HALKYARD 2000 *Journal of Sound and Vibration* **230(3)**, 561-589. Time Domain Estimation of Response and Intensity in Beams Using Wave Decomposition and Reconstruction.
- 5- B. R. MACE 1984 *Journal of Sound and Vibration* **97(2)**, 237-246. Wave Reflection and Transmission in Beams.
- 6- L. JACOBSEN and R. AYRE 1958 *Engineering Vibrations with Applications to Structures & Machinery*. New York: McGraw-Hill.
- 7- P. CLARK 1995. PhD Thesis, *University of Southampton*. Devices for the reduction of pipeline vibration.
- 8- L. CREMER, M. HECKL and E. E. UNGAR 1975 *Structure – borne sound*. New York: Springer – Verlag.
- 9- F. FAHY 1985 *Sound and Structure Vibration*. London: Academic Press.
- 10- H. EL-KHATIB, B. MACE and M. J. BRENNAN 2003 Technical Memorandum **No.903**, University of Southampton – ISVR. Wave reflection and transmission in thin beams in the presence of undamped absorber.
- 11- G. PAVIC 1976 *Journal of Sound and Vibration* **49**, 221-230. Measurement of structure borne wave intensity, Part 1: formulation of the methods.
- 12- B. R. MACE, and C. R. HALKYARD 2001 *Proceedings of the Inter-Noise 2001*, The Hague, the Netherlands, 875-878. Real-time estimation of the flexural wave amplitude in a beam in the presence of a nearfield.
- 13- M. J. BRENNAN 1998 *Journal of Sound and Vibration* **222(3)**, 389-407. Control of flexural waves on a beam using a tunable vibration neutraliser.
- 14- D. J. MEAD 1982 In *Noise and Vibration* (R. G. WHITE and J. G. WALKER, editors) Chapter 9. Ellis Horwood Publishers, Chichester. Structural wave motion.